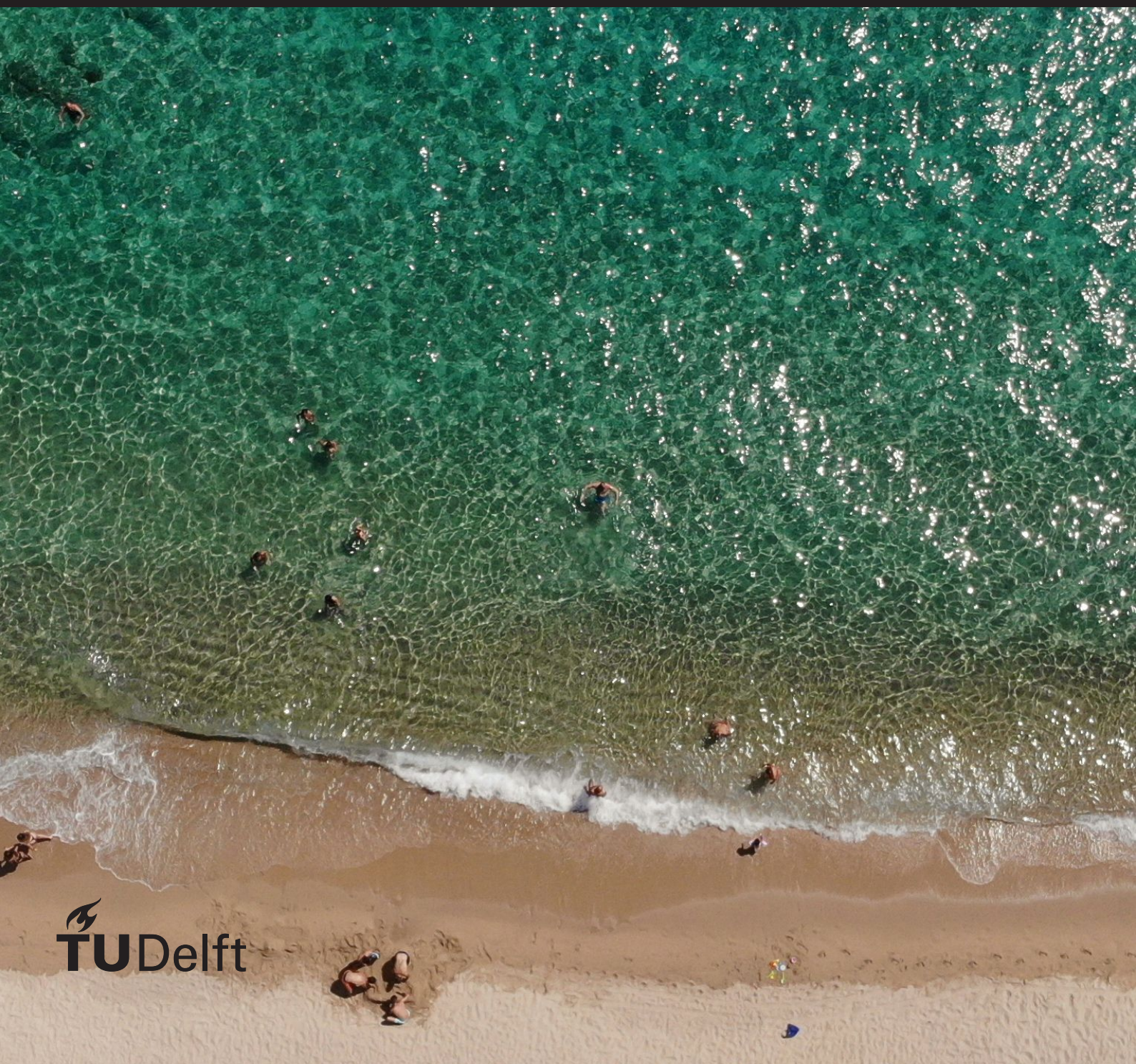
# Investigating Wave Transmission over Submerged Reefs in front of Sandy Beaches as a Nature-Based Coastal Protection Measure

Kashyfi Bin Salleh



TU Delft

# Investigating Wave Transmission over Submerged Reefs in front of Sandy Beaches as a Nature-Based Coastal Protection Measure

by

Kashyfi Bin Salleh

to obtain the degree of Master of Science at the Delft University of Technology, to be defended publicly on Friday July 17, 2026 at 09:00 AM.


| | | |
|---|---|---|
| Student number: | 6288421 | |
| Project duration: | November 11, 2025 – July 17, 2026 | |
| Thesis committee: | Dr. ir. C. Mai Van, | TU Delft, Supervisor |
| | Prof. dr. ir. M.R.A. van Gent, | TU Delft, Deltares |
| | Ir. J. P. van den Bos, | TU Delft, Boskalis |
| | Ir. A.M Korkmaz, | TU Delft |


TU Delft

# Acknowledgements

This thesis marks the conclusion of my MSc studies at TU Delft, and I would like to take this opportunity to thank everyone who supported me along the way. First and foremost, I would like to thank my supervisors, Cong Mai Van, Marcel van Gent, Jeroen van den Bos and Alperen Korkmaz, for their guidance, valuable feedback, and continuous support throughout this project. Their expertise and constructive criticism greatly improved the quality of this work, and I am grateful for the time they invested in our discussions. I would also like to thank Chantal and Jennifer for their assistance during the physical model experiments in the Hydraulic Engineering lab, and for their patience with the many practical challenges that arose during testing. To my friends and fellow students in the Hydraulic and Offshore Structures programme, thank you for the discussions, shared frustrations, and moments of encouragement that made this journey more enjoyable. Finally, I want to thank my family for their unwavering support and encouragement throughout my studies.

Artificial intelligence tools were used to assist with grammar checking and the generation of figures during the preparation of this thesis.

*Kashyfi Bin Salleh*
*Delft, July 2026*

# Abstract

The functionality of existing coastal defence structures designed for depth limited wave conditions are at risk due to climate change. Sea level rise could result in stronger wave loads acting on the shore thus reducing the effectiveness of existing coastal structures. Therefore climate adaptation measures are required to ensure that interventions to protect the coastline do not become obsolete. A viable option is to reduce the wave loads before they arrive to the shore. This can be achieved through either increasing the foreshore via sand nourishments or through the construction of offshore breakwaters to attenuate wave energy. In recent times, sand nourishment has become increasing popular as a soft engineering solution to preserve coastlines. However sand nourishments are not permanent and more sediment has to be deposited at regular intervals depending on the rate of erosion at the coasts. Costs of sand nourishments may also rise to unsustainable levels if sea level rise result in elevated rates of erosion. The construction of artificial reefs in front of nourished beaches brings a twofold benefit: they promote marine life and biodiversity whilst simultaneously acting as submerged breakwaters to dissipate wave energy before it reaches the coast.

The effective design of a dual nature based system consisting of a nourished beach and artificial reefs require proper and accurate understanding of the hydrodynamic processes that occur at the beach and in the coastal waters. It would then be critical to know how the waves would interact with the artificial reefs and subsequently the beach. This study built on previous research to expand the knowledge of the behaviour of waves and their interaction with artificial reefs. Through physical modelling tests, the study investigated whether the distance between the artificial reef and the beach would affect the extent of wave energy dissipation by such structures. This would be quantified by the wave transmission coefficient. The influence of this same distance on structure induced wave setup between the reef and beach will also be studied.

Physical modelling tests were conducted in a wave flume , with a submerged artificial reef tested at three positions relative to a nourished beach, located at distances of 4.80 m, 9.20 m, and 13.70 m from the shoreline. A total of 132 test cases were carried out, varying the significant wave height ($0.08\ m \leq H_{m0} \leq 0.20\ m$), wave steepness ($0.015 \leq s_{m-1,0} \leq 0.040$), and relative freeboard ($-1.875 \leq R_c/H_{m0} \leq 0.625$). Wave transmission and structure-induced wave setup were analysed and compared with existing empirical formulas. Existing literature on wave transmission and structure-induced wave setup has largely focused on low-crested structures with limited consideration of the influence of the distance between the structure and the beach. The use of a permeable low-crested structure in front of a nourished beach, with this distance as a variable, represents a configuration that has not extensively addressed. This study therefore aims to fill this gap in knowledge. . This study has thus provided novel insights into this area.

The results indicate that, within the tested range of conditions, the distance between the artificial reef and the beach does not have a significant influence on the wave transmission coefficient $K_t$ nor on the structure-induced wave setup $\delta/H_{m0}$. The relative freeboard $R_c/H_{m0}$ was identified as the dominant parameter governing wave transmission.

It was concluded that within the tested conditions, designers of artificial reefs placed in front of nourished beaches need not place significant attention on the reef-to-shore distance as a primary design parameter. Instead, greater focus should be placed on the local freeboard, wave climate, and reef geometry, which are the parameters shown to govern the hydrodynamic effectiveness of such structures.

# List of Symbols

| | |
|---|---|
| $B$ | Crest width of structure |
| $D_{n50}$ | Nominal median diameter of rocks used to build the artificial reef |
| $H_{m0}$ | Significant wave height |
| $K_t$ | Wave transmission coefficient |
| $K_r$ | Reflection coefficient |
| $L_p$ | Deepwater wavelength based on peak wave period $T_p$ |
| $L_{m-1,0}$ | Deepwater wavelength based on spectral period $T_{m-1,0}$ |
| $R_c$ | Freeboard |
| $T_p$ | Peak wave period |
| $T_{m-1,0}$ | Spectral wave period |
| $c$ | Wave gauge calibration coefficient |
| $h$ | Local water depth |
| $h_c$ | Crest height of structure |
| $s_{m-1,0}$ | Wave steepness based on spectral period $T_{m-1,0}$ |
| $s_{0m}$ | Deepwater wave steepness |
| $\alpha$ | Angle of structure slope |
| $\delta$ | Wave setup |
| $\rho_b$ | Bulk density |
| $\rho_s$ | Density of rock |
| $\rho_w$ | Density of water |
| $\xi$ | Iribarren number (surf similarity parameter) |
| $\Delta$ | Relative rock density = $\Delta = \frac{\rho_s - \rho_w}{\rho_w}$ |

# List of Figures


2.1 Coastal management strategies. Source: Bosboom and Stive (2021). . . . . 3
2.2 The Sandmotor beach nourishment along the Dutch Coast. Source: Rijkswaterstaat . . 4
2.3 A system of segmented offshore breakwaters. Source: US Army Corps of Engineers . . 5
2.4 Artificial Reefs in Antigua. Source: Reef Beach Shoreline Restoration . . . . . 6

3.1 Theoretical framework. . . . . 12
3.2 Drawing of bed slope installed in the sediment flume (not to scale) . . . . . 13
3.3 Cross sectional drawing of the artificial reef . . . . . 13
3.4 Picture of the artificial reef prior to installation in the flume . . . . . 14
3.5 Picture of amplifier boxes and data acquisition box connected to a computer for data collection . . . . . 15
3.6 Position 1,2 and 3 for the artificial reef along the foreshore slope (not to scale) . . . . . 16
3.7 Position of the wave gauges and EMFs for position 1 . . . . . 16
3.8 Position of the wave gauges and EMFs for position 2 . . . . . 16
3.9 Position of the wave gauges and EMFs for position 3 . . . . . 17
3.10 Drawing of the placements of the cameras . . . . . 17
3.11 View from Go Pro 1: Side Profile . . . . . 17
3.12 View from Go Pro 2: Top view after the reef . . . . . 18
3.13 View from Go Pro 3: Top view before the reef . . . . . 18

4.1 Zoomed in view of the start and end of a raw data time series to indicate regions of calm water without the propagation of waves . . . . . 22
4.2 Four plots visualizing the different steps of the clipping process of raw data to remove periods of calm water at the start and end of the raw time series. . . . . 23
4.3 Placements of the wave gauges for the tests without the reef relative to the three reef positions . . . . . 24
4.4 Evolution of the significant wave height $H_{m0}$ and spectral period $T_{m-1,0}$ as waves travel along the sloped foreshore in the absence of the artificial reef. The x axis values are the distance of the wave gauges relative to Wave Gauge 1. . . . . 24
4.5 Wave energy spectra at Wave Gauge 1 and Wave Gauge 9 for the no-reef tests across three still water depths. The reduction in spectral energy between WG1 and WG9 reflects the natural wave energy dissipation along the flume in the absence of the reef structure. 25
4.6 Two groups of wave gauges are used to decompose wave signal into incident and reflected waves in regions before and after the reef . . . . . 25
4.7 Decomposition of raw measured wave signals into constituent reflected and incident wave signals with their respected spectral significant wave heights $H_{m0}$ . . . . . 26
4.8 Relative positions of the reef for reference . . . . . 27
4.9 Array of Wave Gauges 1,2 and 3 are 72 cm closer to the reef for Position 2 as compared for Positions 1 and 3. The positions of the other wave gauges relative to the reef remain the same . . . . . 27
4.10 Physical model used in the study by Klopman and van der Meer (1999) . . . . . 28
4.11 Comparison of decomposed incident wave height , $H_{m0,inc}$ before the reef for matched test cases across all three reef positions. Only tests with conditions found in the test plans for all 3 positions were plotted to ensure a fair and clean comparison. . . . . 29
4.12 Comparison of reflection coefficient, $K_r$, before the reef for matched test cases across all three reef positions. Only tests with conditions found in the test plans for all 3 positions were plotted to ensure a fair and clean comparison. . . . . 29

4.13 Decomposed incident wave height ($H_{m0,inc}$) against $R_c/H_{m0}$ with artificially generated values for Position 2 tests.Only tests with conditions found in the test plans for all 3 positions were plotted . . . . . 30
4.14 Measured wave transmission coefficient $K_t$ as a function of relative freeboard $R_c/H_{m0}$, grouped by reef position. Left: all test conditions. Right: subset of test conditions with overlapping parameters across all three positions, with a fitted curve. . . . . 31
4.15 The total wave reduction coefficient $K_{total\ reduction}$ is plotted as a function of the relative freeboard $R_c/H_{m0}$ for all test conditions (left). The right plot shows only the subset of test conditions with overlapping parameters across all three reef positions, providing a fairer comparison by considering only tests conducted under the same wave conditions. A fitted curve is also included in the right plot to illustrate the dependency of $K_{total\ reduction}$ on $R_c$. . . . . 32
4.16 The measured wave transmission coefficient $K_t$ is plotted as a function of the relative freeboard $R_c/H_{m0}$ for all test conditions (left). The right plot shows only the subset of test conditions with overlapping parameters across all three reef positions, providing a fairer comparison by considering only tests conducted under the same wave conditions. Both plots are grouped by wave steepness $s_{m-1,0}$, and a fitted curve is included in the right plot to illustrate the overall trend. . . . . 33
4.17 Plot of the ratio of $T_{m-1,0}$ after and before the reef . . . . . 34
4.18 Characteristic changes in spectral shape for before and after the reef. Left: Position 1, Right: Position 3 . . . . . 34
4.19 Measured versus calculated wave transmission using Equation 2.11. The $R_c/H_{m0}$ value used in the equation has been corrected to factor in the setdown that occurs at the reef. 35
4.20 Measured wave transmission coefficient $K_t$ plotted against the values calculated using Equation 2.11 with refitted c1 and c5 coefficients. The new coefficient values are $c_1 = 0.333$, $c_5 = 0.488$. . . . . 36
4.21 Measured wave transmission coefficient $K_t$ plotted against the relative freeboard $R_c/H_{m0}$, with the refitted Van Gent et al. (2023) formula shown as a solid line and the associated 90% confidence interval shown as the shaded region. The formula curve is evaluated at the mean relative crest width $B/L_{m-1,0}$ across all test conditions. . . . . 37
4.22 Top: Raw time series with calm waters at the start used to determine $V_{calm}$. Bottom: Clipped time series with only waves to determine $V_{mean}$ . . . . . 38
4.23 Calculation of actual wave setup $\delta_{actual}$ as a sum of observed wave setup after the reef and observed wave setdown before the reef . . . . . 39
4.24 Plot of non-dimensional structure induced wave setup $\delta/H_{m0}$ against relative freeboard $R_c/H_{m0}$ grouped by position of reef.$R_c/H_{m0}$ has been corrected to factor in the setdown that occurs at the reef. . . . . 39
4.25 Plot of non-dimensional structure induced wave setup $\frac{\delta}{H_{m0}}$ against relative freeboard $\frac{R_c}{H_{m0}}$ grouped by wave steepness. . . . . 40
4.26 Measured setup versus calculated setup based using equation 2.14 . . . . . 41
4.27 Measured vs. calculated $\delta/H_{m0}$ for tests within (left) and outside (right) the valid range of Equation 2.14. . . . . 42
4.28 Measured wave setup $\delta/H_{m0}$ plotted against the values calculated using the empirical setup formula with the leading coefficient refitted from 0.22 to 0.289, grouped by reef position. . . . . 43
4.29 Measured vs. calculated $\delta/H_{m0}$ for tests within (left) and outside (right) the valid range of Equation 2.14. . . . . 43
4.30 Measured wave setup $\delta/H_{m0}$ plotted against the relative freeboard $R_c/H_{m0}$, with the optimised setup formula shown as a solid line and the associated 90% confidence interval shown as the shaded region. The formula curve is evaluated at the mean wave steepness $s_{m-1,0}$ and mean relative crest height $h_c/H_{m0}$ across all test conditions. . . . 44

# List of Tables


2.1 Coefficient values of a and b for Equation 2.5 . . . . . 8
2.2 Coefficient values for wave transmission coefficient proposed by Van Gent et al. (2023). 9

3.1 Overview of experimental parameter values tested across all positions. Refer to Appendix C for the complete test log per position. . . . . 19
3.2 Overview of experimental parameter values used for Position 1 tests. . . . . 20
3.3 Overview of experimental parameter values used for Position 2 tests. . . . . 20
3.4 Overview of experimental parameter values used for Position 3 tests. . . . . 20
3.5 Overview of experimental parameter values used for tests with an artificial reef. . . . . 21

4.1 Comparison of test conditions between Klopman and van der Meer (1999) and Position 2 tests . . . . . 28
4.2 Ranges of experiment conditions for those used to fit Equation 2.14 and for this project 42

A.1 Calibration coefficients for the wave gauges used to convert voltage measurements to water surface elevation. . . . . 53

B.1 GoPro camera settings used during the experiments. . . . . 54

D.1 Test log for Position 1 . . . . . 56
D.2 Test log for Position 2 . . . . . 58
D.3 Test log for Position 3 . . . . . 59

# Contents


**1 Introduction** **1**
- 1.1 Research Context . . . 1
- 1.2 Project Motivation and Research Gap . . . 1
- 1.3 Research Aim and Scope . . . 2
- 1.4 Research Objectives . . . 2
- 1.5 Research Questions . . . 2
- 1.6 Research Theory and Methods . . . 2

**2 Literature Review** **3**
- 2.1 Coastal Zone Management . . . 3
- 2.2 Beach Nourishments . . . 4
- 2.3 Submerged Offshore Breakwaters . . . 5
- 2.4 Artificial Reefs . . . 6
- 2.5 Wave Reflection . . . 7
- 2.6 Wave Transmission . . . 8
- 2.7 Structure Induced Wave Setup . . . 9
- 2.8 Revisiting Project Motivation and Research Gap . . . 10

**3 Methodology** **12**
- 3.1 Theoretical Framework . . . 12
- 3.2 Overview . . . 13
- 3.3 Physical Model . . . 13
  - 3.3.1 Flume and Bed Slope . . . 13
  - 3.3.2 Artificial Reef . . . 13
  - 3.3.3 Wave Generator . . . 14
  - 3.3.4 Measuring Instruments . . . 14
  - 3.3.5 Video Recording . . . 15
  - 3.3.6 Positioning of Physical Model Elements . . . 15
- 3.4 Test Plan . . . 19
  - 3.4.1 Test plan for Position 1 . . . 20
  - 3.4.2 Test plan for Position 2 . . . 20
  - 3.4.3 Test plan for Position 3 . . . 20
  - 3.4.4 Test plan for without an artificial reef . . . 21
  - 3.4.5 Summary of range of parameters and sources of uncertainty . . . 21

**4 Data Analysis and Results** **22**
- 4.1 Data Pre-Processing . . . 22
- 4.2 Wave Propagation on an Empty Foreshore . . . 24
- 4.3 Decomposition of Wave Signal into Incident and Reflected Waves . . . 25
- 4.4 Wave Transmission Analysis . . . 31
  - 4.4.1 Influence of distance on wave transmission . . . 31
  - 4.4.2 Influence of wave steepness on wave transmission . . . 33
  - 4.4.3 Influence of other parameters on wave transmission . . . 33
  - 4.4.4 Transformation of spectral wave period $T_{m-1,0}$ . . . 33
  - 4.4.5 Performance of existing empirical formula . . . 35
- 4.5 Structure Induced Wave Setup . . . 38
  - 4.5.1 Influence of distance on structure induced wave setup . . . 39
  - 4.5.2 Influence of wave steepness on structure induced wave setup . . . 40
  - 4.5.3 Influence of freeboard on structure induced wave setup . . . 40
  - 4.5.4 Performance of existing empirical formula . . . 41

**5 Discussion** **45**
5.1 Research Limitations and Sources of Uncertainty . . . 45
5.2 Discussion on Wave Transmission and Structure Induced Wave Setup . . . 45
5.3 Implication on the Implementation of Artificial Reefs . . . 46

**6 Conclusions and Recommendations** **47**
6.1 Conclusions . . . 47
6.1.1 Wave transmission: . . . 47
6.1.2 Structure induced wave setup: . . . 47
6.2 Recommendations . . . 48
6.2.1 Possible areas for future research . . . 48
6.2.2 Physical modelling experiments . . . 48

**A Appendix A: Calibration of Wave Gauges** **53**

**B Appendix B: Go Pro Camera Settings** **54**

**C Appendix C: Calculation of Artificial Reef Porosity** **55**

**D Appendix D: Log sheet of Physical Model Tests** **56**

# 1 Introduction

## 1.1. Research Context

Due to climate change, coastal zones are threatened by rising sea levels (Church et al., 2013), increased frequency of storm surge events (Cid et al., 2016) and a changing wave climate (Hemer et al., 2013; Wang et al., 2014). The rate of global mean sea level rise in 2023 was recorded as approximately 4.5mm/year. If this trend continues, global sea levels are projected to increase by an additional 169mm within the next 30 years (Hamlington et al., 2024). As a result, coastal regions are expected to experience aggravated rates of erosion (Greenslade et al., 2020) as well as higher risks of flooding (Nicholls & Cazenave, 2010). Traditional hard engineering solutions, such as seawalls, revetments and groynes, are losing functionality and may become unsustainable in the long term. These structures are also known to potentially leave negative impacts on the surrounding environment (Schoonees et al., 2019). Furthermore, their construction and maintenance costs are much higher as compared to soft engineering solutions like beach nourishments (Hoffman, 2016; Leatherman, 1996). Beach nourishments are currently the favoured approach against erosion of sandy beaches (Hanson et al., 2002). However its effectiveness is threatened by sea level rise which is causing greater wave energy forcing on shorelines (Parkinson & Ogurcak, 2018). As a result there has been a resurgence in the interest of using multiple coastal structures in tandem such as the perched beach system. The construction of offshore breakwaters to reduce wave loads to increase the longevity of nourished beaches is a combination system that has been identified as a viable climate adaptation measure (Dinu et al., 2025).

## 1.2. Project Motivation and Research Gap

Artificial reefs are defined as man made underwater obstructions that are located beneath the sea surface level. Artificial reef breakwaters are a variant of conventional submerged offshore breakwaters, with the additional purpose of promoting marine ecology (Bohnsack & Sutherland, 1985) alongside their primary function of attenuating wave energy and reducing wave forces at the shoreline (Pilarczyk, 2003). Incident waves are partially reflected at the reef structure, whilst larger waves are forced to break over the crest. Beach nourishment has become a prevalent soft engineering measure for combating the effects of structural coastal erosion, including shoreline retreat and the progressive narrowing of beach widths. Effective and successful coastal zone management efforts require a deep understanding of coastal processes which includes the interaction of hydrodynamic processes with the beach geomorphology. Hence there is a need to study such processes and interactions in order to formulate successful and long lasting solutions. Sustainable development is also a key focus within coastal zone management, thus obtaining greater understanding of the behaviour of dual nature based solutions such as artificial reef breakwaters in tandem with sand nourishments is of great interest for its implementation.

## 1.3. Research Aim and Scope

The research aim is to obtain a better understanding of the interaction between coastal hydrodynamic processes and coastal protection structures. Specifically, how the distance between an offshore artificial reef breakwater structure and a nourished beach affects wave transmission over the structure and the resulting structure induced wave setup in the inter-structure region.

## 1.4. Research Objectives

1. To set up a physical experiment in a wave flume to study wave transmission over submerged reefs on a sandy beach.
2. To assess the effectiveness of combined artificial reefs and sand nourishment in reducing wave loads on coastal zones.
3. To provide empirical relations and formulations that can inform the design and implementation of nature-based coastal protection measures.

## 1.5. Research Questions

1. To what extent does the distance between artificial reefs and nourished beaches affect the wave transmission over the reefs?
2. To what extent does the distance between artificial reefs and nourished beaches affect the structure induced wave setup between the reefs and the beach?
3. How can existing empirical equations be adapted to factor in these effects (if any)?

## 1.6. Research Theory and Methods

This research utilised physical model experiments in a wave flume to investigate the effectiveness of submerged reefs and sand nourishment in reducing wave loads.

- Hydraulic parameters that were varied: water depth, wave height and wave steepness.
- Physical parameters that were varied: position of the submerged reef.

This study built upon existing literature on the phenomena of wave transmission, including empirical expressions and observed trends between certain hydraulic and geometric variables. Measured data was processed and analysed to obtain quantitative values describing the interaction between coastal hydrodynamics and coastal structures. Data from this project was then evaluated with existing formulas from the literature (Van Gent et al., 2023).

The structure of this thesis is as follows. Chapter 2 discusses relevant studies and existing knowledge of different coastal management measures, wave transmission, wave reflection and structure induced wave setup. Chapter 3 explains the research methodology of this study which includes the physical model and data acquisition methods. Chapter 4 presents the analysis of the experimental data, investigating the influence of the distance between an artificial reef and a nourished beach on wave transmission over the reef structure and the structure-induced wave setup in the inter-structure region. Chapter 5 discusses the implications of the findings from the previous chapter. The chapter addresses possible adaptations to existing empirical formulas and the impact on artificial reef design and construction. The thesis concludes with Chapter 6 which lays out recommendations for future studies.

# 2

# Literature Review

## 2.1. Coastal Zone Management

Coastal zone management is an extensive and multi-disciplinary effort with the primary objective of holistically managing dynamic coastal systems. On a larger scale, coastal zone management considers all factors which has an influence on the future of the coastal zone. This includes environmental protection, politics, policy making and economics (Clark, 2018). All while placing great focus on sustainable development. Coastal zone management encompasses numerous scientific and engineering disciplines beyond coastal engineering alone. It involves processes that occur both at the beach and further away from the shore. For example, coastal systems may suffer from sediment deficit and structural erosion due to constructions of dams in rivers upstream (Syvitski et al., 2005). A major role of coastal management is to carefully evaluate and seek compromise between the mentioned factors.

Successful and effective coastal management can only be achieved when there is thorough understanding of the coastal processes that occur. This refers to the interaction between hydrodynamic factors like waves, wind, tides and currents and the geological factors such as sediment types and local bathymetry.

Coastal management strategies to address coastal erosion can be categorised into three broad groups (Bosboom & Stive, 2021).

1. Retreat: Accept the effects of coastal erosion, do nothing and retreat further inland.
2. Accommodate: Adapt infrastructure along the coasts to be more resilient against the risks of erosion and flooding.
3. Protect: Implement protective measures against erosion and flooding.

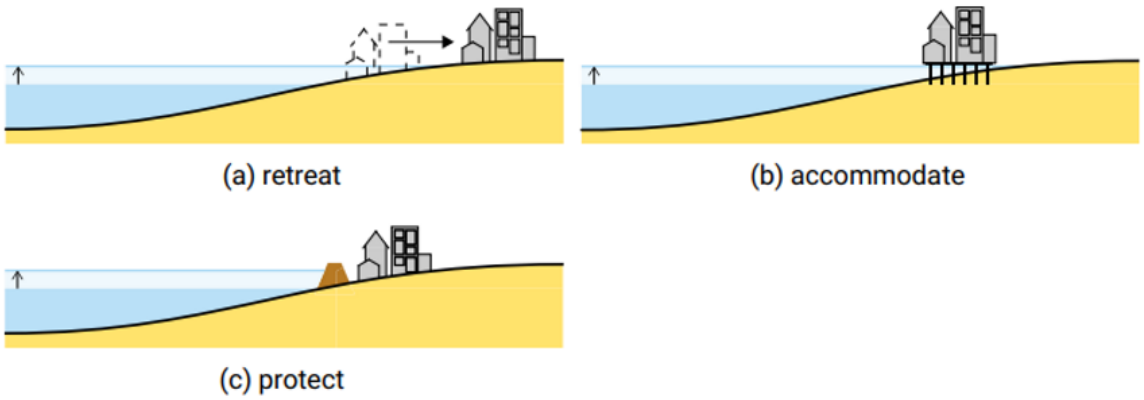



Figure 2.1: Coastal management strategies. Source: Bosboom and Stive (2021).

The tools available to coastal engineers in coastal management consists of cross shore structures such as jetties and groynes, shore parallel structures like breakwaters, revetments, seawalls and dikes and other measures like beach nourishments (Bosboom & Stive, 2021; CIRIA et al., 2007). These measures can be applied in isolation or in combinations with one another depending on the specific needs of the project.

## 2.2. Beach Nourishments

Beach nourishments, also known as shore nourishments, is a soft engineering solution whereby sand is imported and placed along a stretch of coast that is sediment starved. It is in contrast to measures which try to counteract the natural processes causing the erosion. They are carried out on sandy beaches and coastal zones with the aim of preventing shoreline retreat and to maintain beach widths (Dean, 2003).

Sand nourishments are favoured as a coastline management strategy as it maintains and creates spaces by the coast for recreational use. It is also associated with comparatively fewer adverse environmental impacts than traditional hard engineering solutions such as groynes, seawalls and breakwaters. (Hanson et al., 2002). Sources of sediment for shore nourishments include material by-products from port or river dredging operations or from offshore dredging pits on the seabed. Sand nourishments are carried out on a periodic basis at intervals dependent on erosion rates at the project site (Hanson et al., 2002).



Figure 2.2: The Sandmotor beach nourishment along the Dutch Coast. Source: Rijkswaterstaat

Some examples of beach nourishment projects include the Sandmotor along the Delfland Coast in the Netherlands and along the coastline at Grand Popo in Benin. Sandy beaches have beach face slopes with characteristic slopes of 1:10 to 1:30 depending on sediment grain size (Van Bemmelen et al., 2020).

## 2.3. Submerged Offshore Breakwaters

Offshore submerged breakwaters are breakwater variants which are low crested and located a distance away from the coast. Their orientation can be shore parallel or oblique. Their primary function is to modify and reduce wave loads acting on the adjacent beaches or on the structures attached to the coast. Shore-directed waves are reflected at and break over these structures, resulting in the dissipation of wave energy that would otherwise reach the shoreline (Pilarczyk & Zeidler, 1996). The attenuation of wave energy leads to weaker alongshore currents, which in turn reduces the potential for alongshore erosion. (Bosboom & Stive, 2021). The extent of cross-shore erosion capable of occurring during storms are also diminished.

Unlike cross-shore directed structures like groynes which may result in adverse sediment deficit problems on the downdrift direction (Van Rijn, 2011), properly designed offshore breakwaters may allow for the continued passage of alongshore sediment transport through the project area (Bosboom & Stive, 2021; Pilarczyk & Zeidler, 1996).

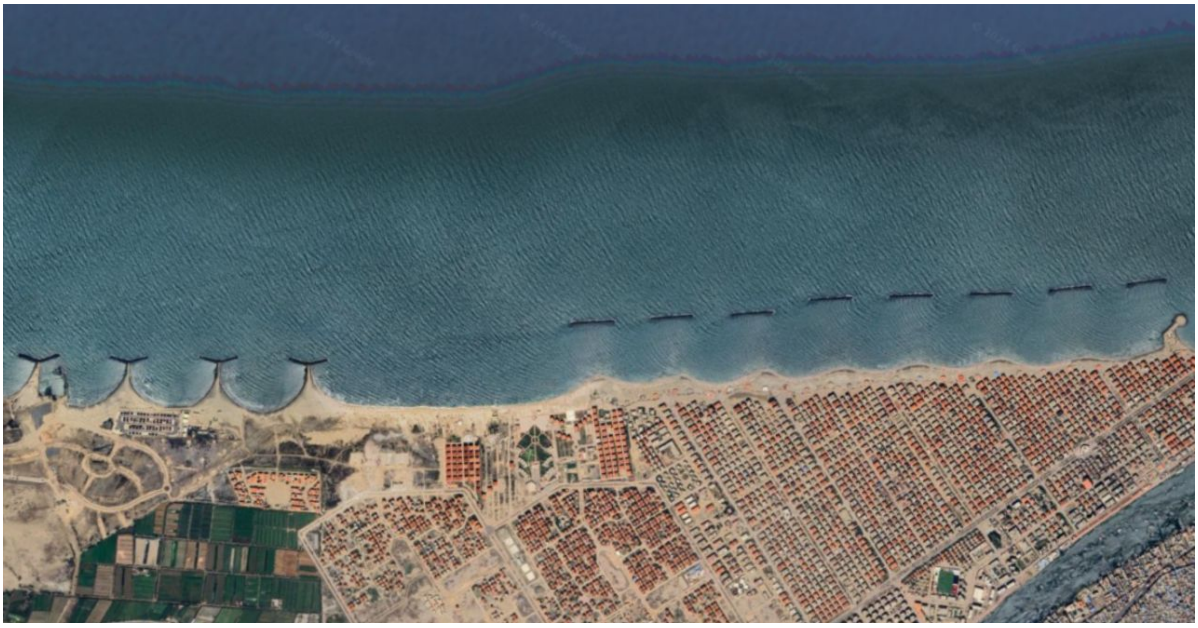


Figure 2.3: A system of segmented offshore breakwaters. Source: US Army Corps of Engineers

Offshore breakwaters can be of two variants: submerged or emerged. Submerged breakwaters are low-crested shore-parallel structures with crests positioned at or below the still water level. Emerged breakwaters, by contrast, have crests that extend above the still water level. Whilst the latter has been observed to be more effective at reducing wave loads, their appearance alongshore is aesthetically unpleasant. Most coastal management committees would opt against choosing emerged offshore breakwaters, especially since beaches are the main tourist attraction for many countries. The implementation of emerged structures along the coast would therefore be detrimental to the local economy. Submerged variants, while not as effective in dissipating wave energy, are more accepted by the public as they remain mostly hidden beneath the water surface. Offshore breakwaters can also be constructed as one continuous structure or in segments.

These structures have been implemented on their own as a way to control shoreline evolution through their ability to redistribute sediment transport patterns and to generate preferred beach features like tombolos or salients. However combinations with other coastal management measures are also commonly implemented. For example, perched beach systems are when the nourishment of sandy beaches are supplemented by the construction of offshore breakwaters (Gallop et al., 2011). In this case, the erosion rate of the nourished beach is slowed down and the longevity and the time period between required nourishments is increased (Chiaia et al., 1992). Offshore breakwaters can also be used in tandem with coastal measures located closer to or at the shoreline, protecting the latter

from more severe wave action (Pilarczyk, 2003). As a result, the main structure located near the coast can be built more economically. For example, Cox and Clark (1992) presented a design for a tandem breakwater system for Lake Michigan which would result in savings of around one million dollars.

The layout design of offshore breakwaters has been the subject of numerous field investigations and laboratory studies. Available literature suggests that submerged breakwaters should generally be positioned at depths of two to five metres. However, the optimal depth is highly site-specific and should be determined through dedicated site investigations (Pilarczyk & Zeidler, 1996). The location of such breakwaters relative to the shoreline depends heavily on the slope of the seabed and the depth of foundation. Most implementations position offshore breakwaters at distances ranging from several tens to hundreds of metres from the shoreline . Increased erosion occurs for submerged breakwaters placed on the seaward side of the breaking line if their crests are lower. For submerged breakwaters placed in the surf zone and within the region of breaking waves, greater scour can be caused if their heights are greater (Pilarczyk & Zeidler, 1996).

## 2.4. Artificial Reefs

Artificial reefs are man-made structures, placed in shallow waters, which can be constructed out of concrete and rock (Baine, 2001). These structures serve dual roles in both coastal protection and the promotion of coastal ecology. Artificial reef structures are able to function as breakwaters to attenuate wave energy (Armono & Hall, 2003),to control coastal erosion (Harris, 2009) and to supplement fisheries to increase the harvest of algae, fishes, lobster and other shellfish (Bohnsack & Sutherland, 1985). However, the structure's effectiveness in carrying out these functions is dependent on the material used in its construction, the physical geometry of the structure and the suitability of the chosen implementation site (Lokesha et al., 2013).



Figure 2.4: Artificial Reefs in Antigua. Source: Reef Beach Shoreline Restoration

Artificial reefs are widely used in the domain of fisheries ecology and management. However, the focus of this thesis is on their application as a coastal protection measure, specifically in the form of artificial reef breakwaters. Traditional rubble mound breakwaters have porosities in the range of 0.3–

0.5, whilst artificial reefs tend to have greater porosities of 0.5–0.8, providing greater void space for the promotion of marine ecology (Huang et al., 2024). Distinction between submerged breakwaters and artificial reef breakwaters can be through their relative submersion value $\frac{h-h_c}{h_c}$, where $h$ is the water depth and $h_c$ is the crest height of the structure. Artificial reef breakwaters can be considered as having relative submersion less than 0.5 (Pilarczyk & Zeidler, 1996).

Artificial reefs may also function as supporting structures for sand nourished beaches by trapping sediment in the upper shoreface and reducing the loss of sediment offshore. This in turn prolongs the periods between subsequent nourishments (da Silva et al., 2022). This would then be useful for locations with limited access to sediments for future nourishments. Careful consideration of site suitability is essential prior to the implementation of artificial reefs, as failure to do so has been identified as a frequent cause of unsuccessful projects (O'Leary et al., 2001). Therefore, as a coastal protection measure, artificial reefs dissipate incoming wave energy thus limiting sediment transport rates, erosion of beaches and the damage of shore positioned structures like dikes and seawalls.

## 2.5. Wave Reflection

Although wave reflection is not the primary focus of this research, it is a highly relevant process that should be understood. Wave reflection occurs when waves propagate into structures resulting in the reflection of the wave energy back towards it propagation source. Understanding wave reflection is crucial for coastal engineers especially for open coasts and at commercial harbours and ports. The extent of the wave reflection can be characterised by the wave reflection coefficient $K_r$ which is the ratio of the reflected wave height and the incident wave height. Existing literature commonly presents $K_r$ as a function of the Iribarren number, $\xi_p$

$$K_r = \frac{H_r}{H_i} = f(\xi_0) \tag{2.1}$$

$$\xi_p = tan\alpha / \sqrt{\frac{H_0}{L_p}} \tag{2.2}$$

in which

- $H_r$ = reflected wave height,
- $H_i$ = incident wave height,
- $\alpha$ = angle of slope of structure,
- $L_p$ = deep water wavelength corresponding to the peak wave period $T_p$

Existing empirical formulae for $K_r$ includes that from Seelig (1983) who proposed the expression,

$$K_r = \frac{a\xi_p^2}{b + \xi_p^2} \tag{2.3}$$

with a = 0.6 and b = 6.6 for conservative approximates for rough permeable slopes and a = 1.0 and b = 5.5 for smooth slopes. Physical model tests with random waves against rock armoured slopes were carried out by Allsop and Channell (1989), the results of which were reanalysed by Postma (1989) to produce the following best fit curve,

$$K_r = 0.125\xi_p^{0.73} \qquad \sigma(K_r) = 0.060 \tag{2.4}$$

However the applicability of these formulas were restricted to the type of materials and slopes that were used in their respective model tests. The range of wave conditions in which Equation 2.4 is applicable is given by: $0.004 < s_{0m} < 0.052$ and $0.6 < \frac{H_s}{\Delta D_{n50}} < 1.9$ . Where $s_{0m}$ is the deepwater wave steepness and $\Delta$ is the relative rock density . Zanuttigh and Van der Meer (2007) then proposed a new formula that is able to take into account a wider variety of slope types which is given by

$$K_r = tanh(a * \xi^b) \tag{2.5}$$

The calibrated values of the coefficients a and b can be found in Table 2.1 for different slope types.

Table 2.1: Coefficient values of a and b for Equation 2.5

| | a | b |
|---|---|---|
| Rock permeable | 0.12 | 0.87 |
| Armour units | 0.12 | 0.87 |
| Rock impermeable | 0.14 | 0.90 |
| Smooth | 0.16 | 1.43 |

## 2.6. Wave Transmission

Wave transmission is the process by which a wave passes through a medium or moves from one medium to another. In the context of offshore breakwaters, it can be characterized by the wave transmission coefficient, $K_t$, which is the ratio between the transmitted and incident wave heights.

$$K_t = \frac{H_{m0,t}}{H_{m0,i}} \tag{2.6}$$

where $H_{m0,i}$ is the significant wave height of the incident waves in front of the breakwater and $H_{m0,t}$ is the significant wave height of the transmitted waves at the rear side of the breakwater. The wave transmission coefficient is a quantifiable parameter used to assess the effectiveness of breakwaters in reducing wave loads on the shore. Wave transmission has been studied extensively by numerous researchers with many yielding empirical equations to quantify $K_t$. Most of these studies were physical model experiments that involved wave transmission over low-crested structures. Laboratory tests by Daemen (1991) led to Equation 2.7 for wave transmission over trapezoidal rubble mound breakwaters.

$$K_t = \left(0.031\frac{H_{m0}}{D_{n50}} - 0.024\right)\frac{R_c}{D_{n50}} + \left(0.51 - 5.42s_{op} + 0.0323\frac{H_{m0}}{D_{n50}} - 0.0017\left(\frac{B}{D_{n50}}\right)^{1.84}\right) \tag{2.7}$$

d'Angremond et al. (1996) conducted further experiments and proposed Equation 2.8 for wave transmission over impermeable and permeable structures.

$$K_t = -0.4\frac{R_c}{H_{m0}} + c\left(1 - e^{-0.5\xi_{op}}\right)\left(\frac{B}{H_{m0}}\right)^{-0.31} \tag{2.8}$$

d'Angremond's expression was subsequently adapted by Briganti et al. (2003) to produce Equation 2.9. This adapted expression is able to account for wave transmission over permeable structures with wide crests ($B/H_{m0} > 10$).

$$K_t = -0.35\frac{R_c}{H_{m0}} + 0.51\left(1 - e^{-0.41\xi_{op}}\right)\left(\frac{B}{H_{m0}}\right)^{-0.65} \quad \text{for } \xi_{op} < 3 \tag{2.9}$$

Van der Meer et al. (2005) followed up by proposing Equation 2.10 for wave transmission over permeable structures with very wide crests ($B/H_{m0} > 12$).

$$K_t = -0.3\frac{R_c}{H_{m0}} + 0.75\left(1 - e^{-0.5\xi_{op}}\right) \quad \text{for } \xi_{op} < 3 \tag{2.10}$$

The inclusion of variables such as the freeboard $R_c$, the significant wave height $H_{m0}$, crest width $B$, and wave steepness $s$ (embedded in the breaker parameter $\xi$) in the proposed expressions indicate their influence on wave transmission. However, the results from these studies were obtained by different researchers in different laboratories through a myriad of different methodologies. Furthermore, the data from these previous studies do not form a homogeneous database. Although common trends with

respect to the key variables were observed across the earlier empirical expressions, their predictive performance was found to be inadequate when applied outside their original range of validity.

In response, Van Gent et al. (2023) carried out extensive physical model tests, with different wave heights and steepnesses, to study wave transmission over impermeable, permeable and perforated structures. This resulted in Equation 2.11 with the coefficient values given in Table 2.2.

$$K_t = c_1 \tanh\left(-\left(\frac{R_c}{H_{m0}} + c_2\left(\frac{B}{L_{m-1,0}}\right)^{c_3} + c_4\right)\right) + c_5 \tag{2.11}$$

Table 2.2: Coefficient values for wave transmission coefficient proposed by Van Gent et al. (2023).

| Structure type | $c_1$ | $c_2$ | $c_3$ | $c_4$ | $c_5$ | RMSE |
|---|---|---|---|---|---|---|
| A: Impermeable structure | 0.47 | 3.1 | 0.75 | 0 | 0.50 | 0.0166 |
| B: Permeable structure (rubble mound structure) | 0.43 | 3.1 | 0.75 | −0.25 | 0.50 | 0.0198 |
| C: Perforated structure | 0.13 | 3.1 | 0.75 | −0.15 | 0.82 | 0.0149 |
| D: Perforated structure with screen | 0.40 | 3.1 | 0.75 | −0.15 | 0.50 | 0.0229 |
| E: Perforated structure with perforated screen | 0.17 | 3.1 | 0.75 | −0.15 | 0.76 | 0.0137 |

This new expression has a range of validity for permeable structures with dimensionless crest level values of $-2.5 \leq R_c/H_{m0} \leq 2.5$ and dimensionless crest width values of $0.9 \leq B/H_{m0} \leq 10.6$. Equation 2.11 performed relatively well when used to predict $K_t$ using datasets by Daemen (1991) and Calabrese et al. (2003) which involved permeable structures. However, for impermeable and perforated structures, the expression is only considered valid for submerged structures.

The conclusions of Van Gent et al. (2023) were consistent with earlier observed trends, confirming that wider crests lead to lower wave transmission, although Van der Meer et al. (2005) noted that this reduction becomes negligible for extremely wide crests ($B/H_{m0} > 12$). Higher wave steepness was similarly found to reduce wave transmission, with the effect being more pronounced for impermeable structures in comparison to permeable structures. Since wave steepness primarily governs wave breaking, its influence on transmission is most significant for slightly submerged structures and diminishes with increasing submergence.

The results from these studies concluded that the primary factors influencing wave transmission are the freeboard, the crest width, the wave height and the wave steepness. These can clearly be seen in their inclusion in the derived empirical equations . The distinction between permeable and impermeable structures is accounted for through the use of different coefficient values seen in Table 2.2. Other factors such as slope of the structure, porosity of the structure, local water depth and stone diameter ($D_{n50}$) were also considered but their effects proved to be not as consequential. Submerged structures can be categorized as slightly or more submerged based on the value of their freeboard $R_c$.

However the influence of the distance between the offshore structures and the shoreline was not investigated by these tests and remain poorly understood. This thesis addresses this gap in knowledge through physical modelling tests in a wave flume.

## 2.7. Structure Induced Wave Setup

Structure induced wave setup, also known as the piling up of the water that overtops a breakwater, refers to the increase in the mean water level in the shore side of offshore breakwaters. Pilarczyk and Zeidler (1996) explains that the energy of the water that overtops the structure creates secondary waves within the protected region behind the breakwater. At the same time, the water that passes the breakwater also piles up within the same region. This generates a difference in the mean water level between the area behind the breakwater and that of the open sea. When there is a steady supply of incoming waves, the piling up of water becomes substantial enough to maintain equal rates of inflow and outflow across the breakwater thus maintaining the elevated water levels.

This phenomenon has been studied by Longuet-Higgins (1967) who described an analytical solution under the simplified scenario of non breaking, small amplitude monochromatic waves whilst ignoring the effects of friction on structures. Diskin et al. (1970) followed up by conducting physical experiments using monochromatic waves thus deriving the empirical Equation 2.12. In this formula, it is indicated that the non dimensional wave induced setup $\frac{\delta}{H}$ is dependent only on the non dimensional freeboard $\frac{R_c}{H}$.

$$\frac{\delta}{H} = 0.6e^{-[(0.7-\frac{R_c^2}{H})]} \tag{2.12}$$

Loveless et al. (1999) then carried out tests with homogenous permeable structures with submerged and emerged crests. It was then concluded that the maximum structure induced setup occurs when the water depth is at the crest, corresponding to a freeboard of zero ($\frac{R_c}{H} = 0$). This is in contrast with Diskin et al. (1970) whose results indicated maximum structure induced setup occurring at $\frac{R_c}{H} = 0.7$ instead. These experiments further concluded that structure-induced wave setup is also influenced by wave height, wave period, local wavelength, water depth in front of the structure, freeboard, crest width, stone diameter and the total height of the structure.

Van Gent (2024) conducted flume experiments investigating the wave setup induced between a low-crested structure and a shore-side emerged structure. Both permeable and impermeable low crested structures were tested in combination with permeable and impermeable shore-side structures. For impermeable low crested structures, a clear dependency on wave steepness was observed. However the distance between both structures showed negligible effect on the induced setup. An empirical relation for impermeable submerged low crested structures in front of another structure was formulated as Equation 2.13.

$$\frac{\delta}{H_{m0}} = 0.34\, s_{m-1,0}^{0.4} \left(\frac{R_c}{H_{m0}} + 1.6\right)^{3.5} \tag{2.13}$$

For permeable structures, there was a less pronounced dependency on wave steepness. However a slight influence of the height of the low crested structure $h_c$ was observed. The influence of distance between both structures were not investigated for permeable low crested structures. An empirical equation for permeable homogeneous submerged low-crested structures in front of a permeable or impermeable structure was formulated as

$$\frac{\delta}{H_{m0}} = 0.22\, s_{m-1,0}^{0.2} \left(\frac{h_c}{H_{m0}}\right)^{-0.7} \left(\frac{R_c}{H_{m0}} + 1.5\right)^{1.5} \tag{2.14}$$

.

However the influence of distance between an offshore low crested structure and the shore was not investigated for permeable low crested structures. This thesis addresses this gap in knowledge through physical modelling tests in a wave flume.

## 2.8. Revisiting Project Motivation and Research Gap

As the effects of climate change and sea level rise become increasingly pronounced, certain coastal protection structures which were designed in depth limited conditions are at risk of losing functionality. Rise in sea level increases the wave heights and wave loads that reach the shoreline and the implementation of offshore submerged breakwaters in front of these existing structures to dissipate wave energy is a solution that is becoming more attractive (Van Gent, 2019; Van Gent & Teng, 2023). As mentioned before, successful coastal zone management requires a deep and insightful knowledge of the coastal processes that occur. Hence it is with great interest that studies are carried out to further the current understanding of the processes related to the implementation of offshore submerged breakwaters in tandem with a nourished beach.

This research investigates how the distance between an offshore permeable low-crested structure and a nourished beach affects wave transmission over the structure and the resulting structure induced wave setup in the inter-structure region. Van Gent (2024) had addressed the influence of the distance

between a low crested structure and the shore for impermeable low crested structures. However the the influence of distance for permeable low crested structures remain inadequately understood. Covering this gap in knowledge is critical for the implementation of artificial reef breakwaters as such structures are permeable in nature. Knowledge on the influence of the distance would be useful in the design of offshore breakwaters, particularly in the choice of how far from the shore such structures should be constructed to obtain optimal reduction of wave loads.

# 3

# Methodology

## 3.1. Theoretical Framework

From the literature review we have found that the influencing factors for wave transmission include,

1. Freeboard over the structure,
2. Significant wave height,
3. Crest width of the structure,
4. Wave steepness.
5. Permeability (and porosity) of structure

In this research, by measuring the water levels in different locations we determined the following variables

1. Incident wave height in front of the structure $H_{m0,incident}$,
2. Transmitted wave height at the rear of the structure $H_{m0,transmitted}$,
3. Wave transmission coefficient $K_t = \frac{H_{m0,transmitted}}{H_{m0,incident}}$
4. Structure induced wave set-up between the low crested structure and the impermeable beach $\delta$.

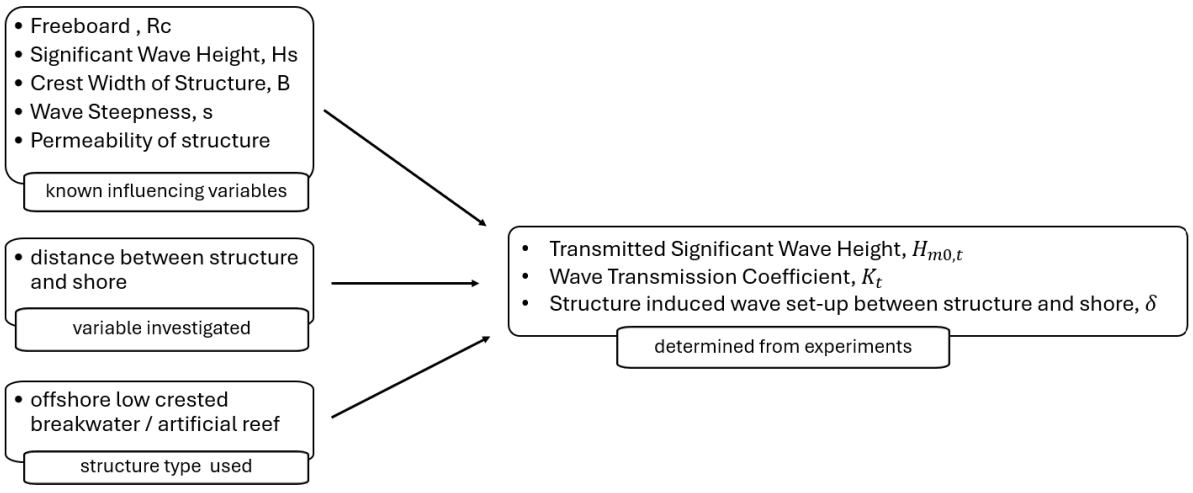



Figure 3.1: Theoretical framework.

A basic form for this study's theoretical framework can be seen in Figure 3.1, which outlines the different variables that were changed throughout the physical model tests to determine the final effect on wave transmission and structure induced wave setup.

## 3.2. Overview

This research project made use of a physical model inside a wave flume to study wave transmission and structure induced wave setup. A piston-type wave generator was used to propagate waves inside the flume and over an artificial reef. Wave heights were measured using wave gauges placed along the flume. Data obtained were studied and analysed to determine the influence of different wave parameters and the position of the reef wave transmission and structure induced wave setup.

## 3.3. Physical Model

### 3.3.1. Flume and Bed Slope

The tests were performed using a wave flume located at the Hydraulic Engineering Lab at Delft University of Technology (TU Delft). The wave flume has a length of 39m, a width of 0.76m and a height of 0.85m. It is equipped with a piston-type wave generator equipped with an active reflection compensator.

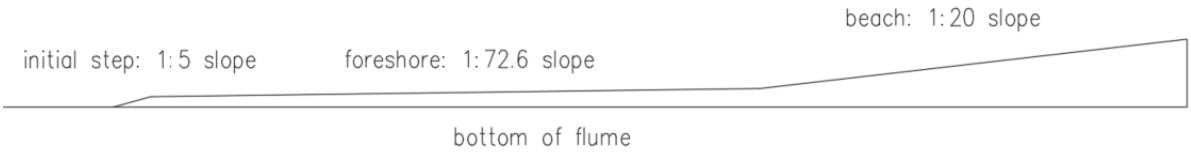



Figure 3.2: Drawing of bed slope installed in the sediment flume (not to scale)

As seen in Figure 3.2, the bed slope of the physical model was constructed from wood and consists of 3 segments. The initial step with a slope of 1:5, a foreshore with a slope of 1:72.6 and a beach with a slope of 1:20.

### 3.3.2. Artificial Reef

The artificial reef was constructed by gluing stones of $D_{n50} = 0.04$ m together to prevent any displacement of its material. The permeability of the structure remained unaffected by the glueing process. It is prismatic and trapezoidal in shape with a base length of 140 cm, a crest width of 35 cm and a crest length as wide as the flume of 76 cm. Its sides have a slope of 2:3 and a base with a slope of 1:72.6 so that the crest remains parallel with the water surface. A cross sectional drawing and a picture of the reef can be seen in Figure 3.3 and Figure 3.4 respectively. Results from the physical model tests are expected to be applicable for structures in the range of about 12 to 15 times larger in reality.

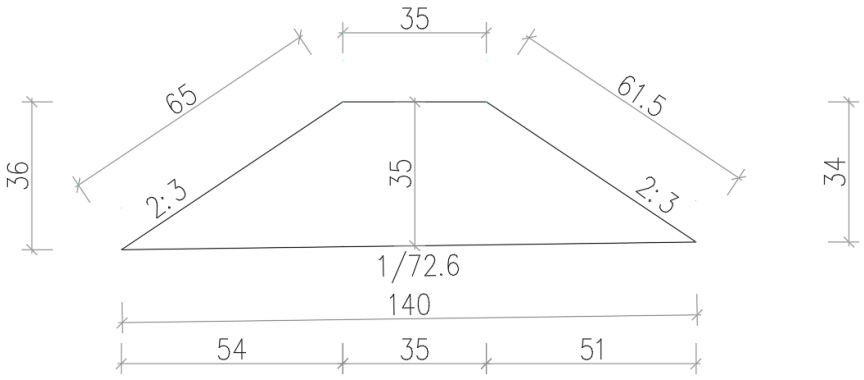



Figure 3.3: Cross sectional drawing of the artificial reef



Figure 3.4: Picture of the artificial reef prior to installation in the flume

The porosity of the reef was calculated to be $0.405$. The method used to determine this value is explained in Appendix C.

### 3.3.3. Wave Generator

The wave generator in the sediment flume has active reflection compensation to account for short waves and long waves effects. This means that the paddle motion adjusts to absorb the waves reflected from the structure and prevent their re-reflection back into the flume.

### 3.3.4. Measuring Instruments

Wave gauges were used to measure the water levels in the flume throughout the experiments. Additionally, electromagnetic flow meters (EMFs) were used to measure the current velocity at regions after the artificial reef. Velocity data measured by the EMFs were not analysed in this project and will instead be used to validate a numerical model in a separate study.

The final physical model configuration uses 9 wave gauges and 4 EMFs positioned at various locations along the flume. The measurement frequency for both the wave gauges and EMFs was 100 Hz. All the wave gauges were calibrated prior to the start of the experiment. The calibration process and calibration coefficients for each wave gauge can be found in Appendix A. Each wave gauge and EMF is connected to an amplifier box which is then connected to a data acquisition module which is subsequently connected to a computer. The software DASYLAB is then used to collect and manage

the data measured during the tests.



Figure 3.5: Picture of amplifier boxes and data acquisition box connected to a computer for data collection

### 3.3.5. Video Recording

Three Go Pro Hero 10 cameras were used to capture video footage of the behaviour of the waves. This footage however was not used directly for this project but instead will be used for future research. The aim of this setup is to capture clear visual data for the analysis of wave behaviour propagating over a reef. The capturing of the footage will be synchronized with the measurements by the wave gauges and EMFs. Calibration to convert pixels in the footage into physical length units ($cm\ or\ mm$) can be carried out with the aid of a grid board attached or drawn onto the side of the wave flume with known scale marks.

One camera was placed perpendicular with the side window of the flume to capture the 2D wave profile (height and period) and the interaction with the artificial reef. Two cameras were placed above the flume, at a short distance before and after the reef and angled downwards towards the crest of the structure. This is to obtain additional visual data on wave patterns and breaking types across the flume width over the reef. The placements of the cameras are visualized in Figure 3.10. Only 15 minutes of footage was captured for each run, starting from when the waves were observed to have stabilized. To allow for a greater distinction between the waterline and the clear background of the flume side panels, white paper sheets or translucent privacy film was fixed to the clear side windows of the flume. Sufficient lighting was provided such that the waterline would appear darker as compared to the brightened background. The settings used for the Go Pro cameras can be found in Appendix B.

### 3.3.6. Positioning of Physical Model Elements

The physical model elements here refer to the wave gauges, the EMFs, the Go Pro cameras and the artificial reef. The artificial reef was positioned at three different locations along the foreshore henceforth referred to as Positions 1, 2 and 3. Position 2 is closer to the beach, Position 3 is closer to the wave machine and Position 1 is in between the other two locations.The different positions are visualized in Figure 3.6. This was to investigate any potential influence of the distance between reef and the beach on the wave transmission and structure induced wave setup.

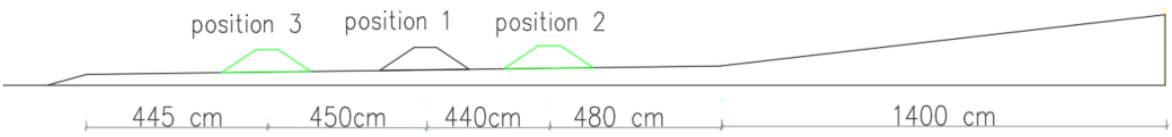



Figure 3.6: Position 1,2 and 3 for the artificial reef along the foreshore slope (not to scale)

An array of 8 wave gauges and 4 EMFs was shifted with the artificial reef as it moved to the 3 positions. These measurement instruments were labelled as Wave Gauges 1,2,3,4,5,6,7,8 and EMF 1,2,3,4. A final wave gauge, Wave Gauge 9 remained fixed at the beach slope for all the experiments regardless of the reef position. Wave Gauge 1,2,3 was used to decompose the measured wave data into incident and reflective waves before the reef while Wave Gauge 6,7,8 was used for decomposition of waves after the reef. For the EMF pairs which are co-located along the flume, one of the EMFs had its probe at a deeper depth to obtain velocity data at different vertical points. As such, EMF 1 and EMF 3 had a deeper probe depths as compared to EMF 2 and EMF 4 respectively.

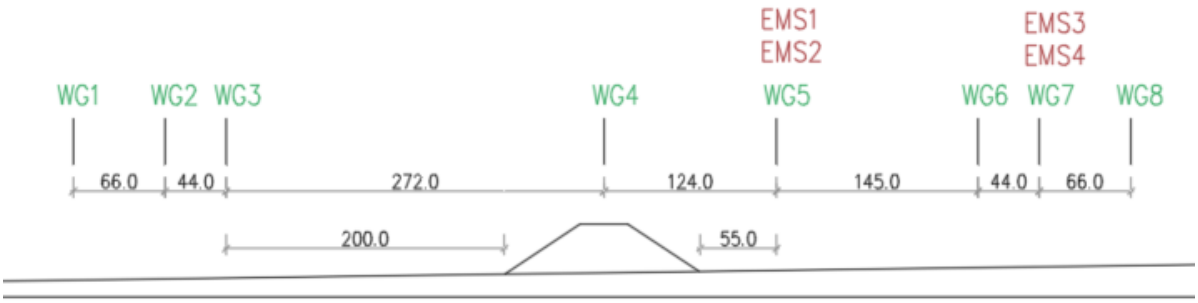



Figure 3.7: Position of the wave gauges and EMFs for position 1

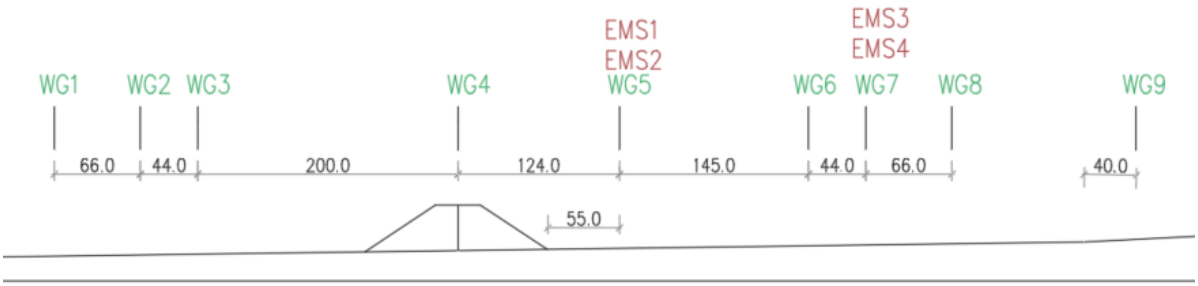



Figure 3.8: Position of the wave gauges and EMFs for position 2

Due to an oversight when marking the positions of the wave gauges along the flume, Wave Gauges 1,2,3 were placed 72 cm closer to the seaward toe of the reef for Position 2 as compared to that for Positions 1 and 3. The applicability of the Position 2 test results was therefore compromised. However,, the relative positions between Wave Gauges 1,2,3 throughout all 3 positions remained constant. The consequence of this difference in distance to the reef for Position 2 tests is explored further in the chapter on Data Analysis and Results.

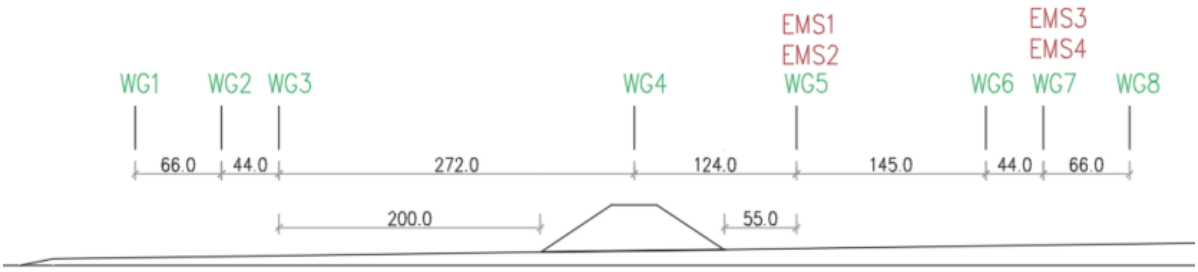



Figure 3.9: Position of the wave gauges and EMFs for position 3

At every position, three Go Pro cameras were installed in fixed positions. One to record the the side view of the reef and two to record top views of the reef. Of the two top views, one camera captured the wave behaviour before the reef and one captured the wave behaviour after the reef.

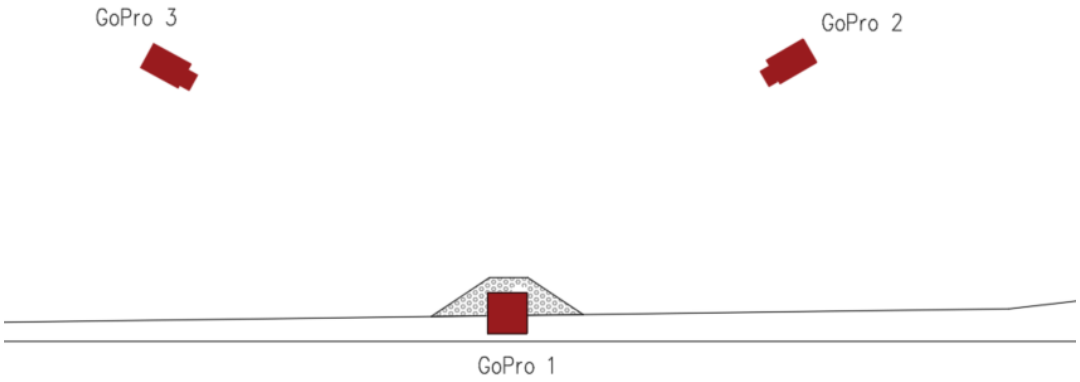



Figure 3.10: Drawing of the placements of the cameras



Figure 3.11: View from Go Pro 1: Side Profile

The three positions of the reef were specifically chosen to be centralised with regards to the clear side panels of the flume to allow unobstructed capturing of wave interaction with the reef by the Go Pro cameras.

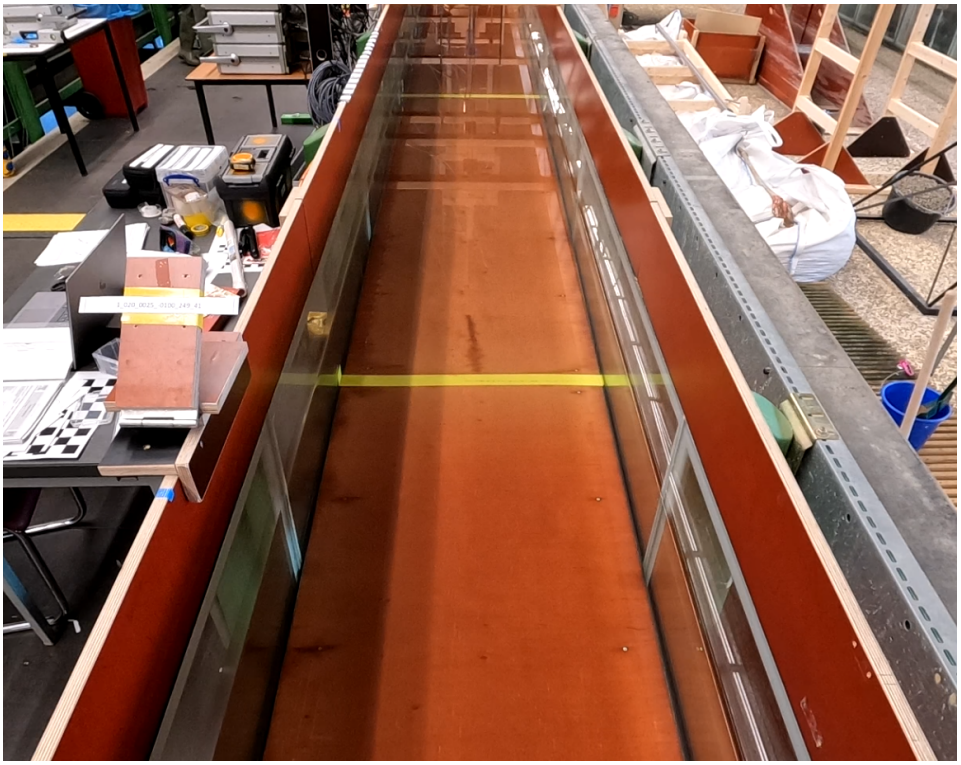


Figure 3.12: View from Go Pro 2: Top view after the reef

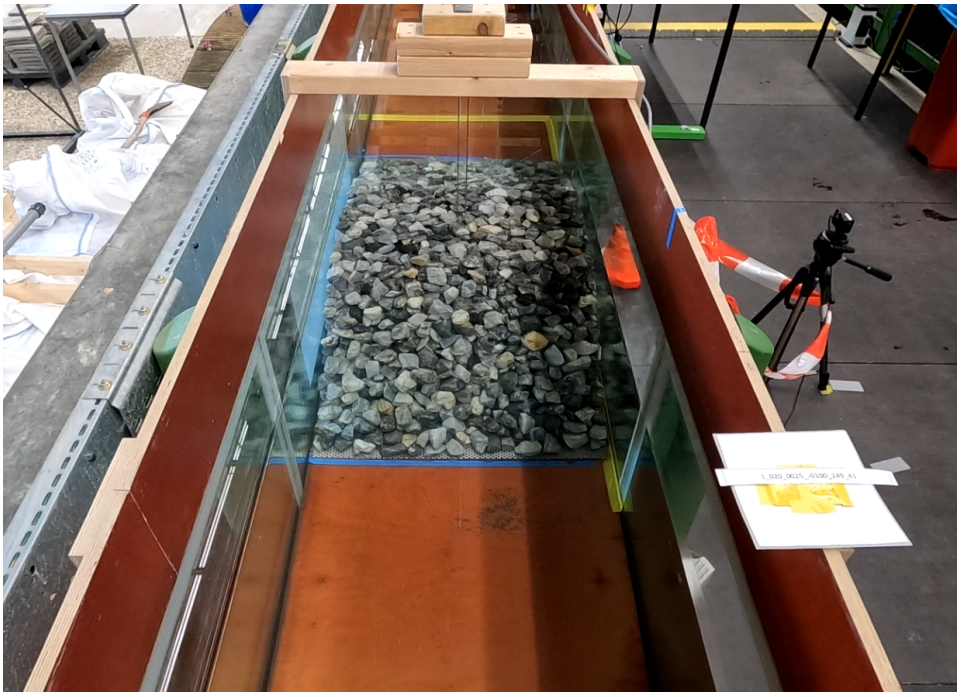


Figure 3.13: View from Go Pro 3: Top view before the reef

## 3.4. Test Plan

The final test plan of the physical model experiment consisted of 132 different runs with varying test conditions as outlined in Table 3.1 and Table 3.5. 129 runs were with an artificial reef installed and three runs were without an artificial reef. The purpose of carrying out experiments without the reef was to act as a control and investigate the interaction of the waves solely with the foreshore and the beach in the absence of any structures. The varied parameters were

1. position of the artificial reef
2. the significant wave height $H_{m0}$
3. wave steepness $s_{m-1,0}$
4. freeboard above the reef crest $R_c$.

The original test plan for tests involving the artificial reef included three reef positions, four significant wave heights, three wave steepnesses and six freeboard values totalling to 216 tests. However upon reconsideration of the limited time available with the flume, a revised test plan of 129 runs was developed. In the revised version, the number of tests in Positions 2 and 3 were reduced whilst the number of tests in Position 1 remained as planned. Table 3.1 presents the complete set of parameter values used throughout the experimental programme. It should be noted that the parameter values tested varied between positions, with not all combinations being tested at every position. Position 1 had 72 tests, Position 2 had 30 tests and Position 3 had 27 tests. A comprehensive log sheet of the tests that were carried out for each position can be found in Appendix D

Table 3.1: Overview of experimental parameter values tested across all positions. Refer to Appendix C for the complete test log per position.

| Position | $H_{m0}$ (m) | $s_{m-1,0}$ (-) | $R_c$ (m) |
|---|---|---|---|
| 1 | 0.08 | 0.015 | 0.000 |
| 2 | 0.12 | 0.025 | −0.050 |
| 3 | 0.16 | 0.040 | −0.075 |
| | 0.19 | | −0.100 |
| | 0.20 | | −0.125 |
| | | | −0.150 |

A wave train sequence was generated using the built in software of the wave generator. The waves generation used a JONSWAP spectrum (with the standard peak enhancement factor of 3.3) which required an input significant wave height and peak period value. For a given wave steepness $s_{m-1,0}$, a corresponding value for $T_{m-1,0}$ and $L_{m-1,0}$ value were calculated using Equation 3.1 and Equation 3.2 respectively. The spectral wave period $T_{m-1,0}$ was used as it has been seen to capture the influence of the spectral shape on processes such as wave run-up, wave overtopping and reflection at coastal structures (Van Gent (1999), Dekker et al. (2007)).

$$T_{m-1,0} = \sqrt{\frac{2\pi H_{m0}}{g s_{m-1,0}}} \tag{3.1}$$

$$L_{m-1,0} = \frac{g T_{m-1,0}^2}{2\pi} \tag{3.2}$$

Peak period, $T_p$ is then calculated using Equation 3.3.

$$T_p = T_{m-1,0} * 1.1 \tag{3.3}$$

Second order wave generation was used to prevent spurious waves that arise with first order generation. On average each test would consist of about 900 waves.

### 3.4.1. Test plan for Position 1

Three tests with target conditions of $H_{m0} = 0.2\ m$ and $R_c = 0\ m$ could not be carried out, as the wave generator was unable to generate the required significant wave height at the corresponding water depth. In these cases, the water depth in the flume was too shallow for the wave machine to generate that high of a significant wave height. As such these three cases were carried out with $H_{m0} = 0.19\ m$ instead. 72 tests were carried out with Position 1.

Table 3.2: Overview of experimental parameter values used for Position 1 tests.

| Position | $H_{m0}$ (m) | $s_{m-1,0}$ (-) | $R_c$ (m) |
|---|---|---|---|
| 1 | 0.08 | 0.015 | 0.000 |
| | 0.12 | 0.025 | −0.050 |
| | 0.16 | 0.040 | −0.075 |
| | 0.19 (only for 3 tests) | | −0.100 |
| | 0.20 | | −0.125 |
| | | | −0.150 |

### 3.4.2. Test plan for Position 2

The test plan for Position 2 had a reduced number of significant wave heights and freeboards. The number of significant wave heights tested were decreased from four to three with the removal of $H_{m0} = 0.12\ m$. The freeboards tested were also decreased from six to four with the removal of $R_c = \{-0.075\ m, -0.125\ m\}$. However it was realised that for higher water depths in the flume which corresponds with $R_c = -0.150\ m$, there was a real possibility of the waves overtopping the side walls of the flume. Due to the limitations of the experimental setup as explained above, further tests involving higher significant wave heights of $H_{m0} = \{0.16\ m,\ 0.20\ m\}$ with freeboards of $R_c = -0.150\ m$ were excluded from the test plan. 30 tests were carried out with Position 2.

Table 3.3: Overview of experimental parameter values used for Position 2 tests.

| Position | $H_{m0}$ (m) | $s_{m-1,0}$ (-) | $R_c$ (m) |
|---|---|---|---|
| 2 | 0.08 | 0.015 | 0.000 |
| | 0.16 | 0.025 | −0.050 |
| | 0.20 | 0.040 | −0.100 |
| | | | −0.150 |

### 3.4.3. Test plan for Position 3

The test plan for Position 3 had a reduced number of significant wave heights and freeboards as well. Tests involving $H_{m0} = 0.12\ m$ and $R_c = \{0.000\ m, -0.075\ m, -0.125\ m\}$ were removed. 27 tests were carried out with Position 3.

Table 3.4: Overview of experimental parameter values used for Position 3 tests.

| Position | $H_{m0}$ (m) | $s_{m-1,0}$ (-) | $R_c$ (m) |
|---|---|---|---|
| 3 | 0.12 | 0.015 | −0.050 |
| | 0.16 | 0.025 | −0.100 |
| | 0.20 | 0.040 | −0.150 |

### 3.4.4. Test plan for without an artificial reef

The runs without an artificial reef were carried out with the measuring instruments placed at their corresponding Position 1 locations. It consisted of 3 runs with constant steepness and significant wave height. 3 different water levels in front of the wave generator was used. These water levels are approximately the corresponding water levels for Position 1 tests with $R_c$ values of 0.000 m, -0.100 m and -0.150 m. The test plan for without the artificial reef is summarised in Table 3.5 below.

Table 3.5: Overview of experimental parameter values used for tests with an artificial reef.

| $H_{m0}$ (m) | $s_{m-1,0}$ (-) | Water level in front of wave generator (m) |
|---|---|---|
| 0.08 | 0.040 | 0.527 |
| | | 0.613 |
| | | 0.683 |

### 3.4.5. Summary of range of parameters and sources of uncertainty

This study investigated a permeable low-crested structure in the form of a prismatic trapezoidal artificial reef constructed from glued rocks.The experimental programme covered parameter ranges of $-1.875 \leq R_c/H_{m0} \leq 0.000$, $1.750 \leq B/H_{m0} \leq 4.375$ and $0.026 \leq B/L_{m-1,0} \leq 0.176$, corresponding exclusively to submerged and just-emergent reef configurations. These ranges fall within the validity range of the empirical expression by Van Gent et al. (2023), which was derived for $-2.5 \leq R_c/H_{m0} \leq 2.5$ and $0.9 \leq B/H_{m0} \leq 10.6$.

The sources of uncertainty in this study can be attributed to three main factors: human error during the execution of the physical model experiments and data analysis, inaccuracies arising from faulty or malfunctioning measuring equipment, and the inherent limitations of the model schematisation.

# 4

# Data Analysis and Results

## 4.1. Data Pre-Processing

Raw experimental data were in the form of ASCII files. These then were imported and processed with the Python programming language. Each experiment produced a file containing 13 sets of time series data, nine from wave gauges and four from the EMFs. Analysis on wave transmission and structure induced wave heights will only make use of the wave gauge time series data. Prior to analysis, the raw datasets were screened to identify and remove invalid NaN values and outliers that could have been caused by equipment malfunction. No NaN values were detected across the dataset, with the exception of the WG4 time series. In this case, faulty records were caused by instances of the water level dropping below the wave probe, occurring predominantly during tests with low freeboard values.

Subsequently, in order to accurately execute a spectral analysis of the waves, a time series containing only wave signals is required. However, the raw time series also includes periods of calm water, in the absence of waves, before and after the wave machine was engaged. This can be observed in Figure 4.1.

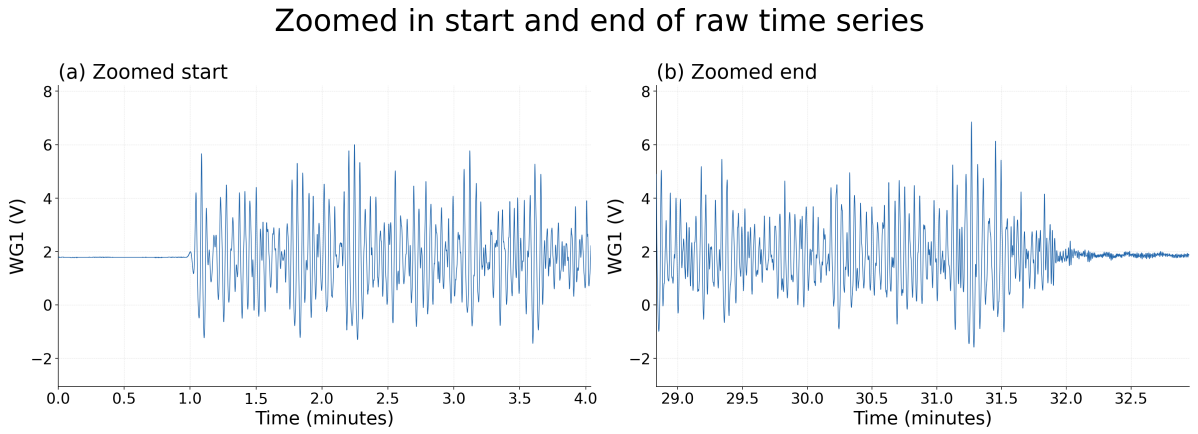



Figure 4.1: Zoomed in view of the start and end of a raw data time series to indicate regions of calm water without the propagation of waves

Clipping of both ends of the data was therefore required and carried out. The process is described below and visualized in Figure 4.2.

1. The mean and standard deviation of the entire time series is calculated.
2. The first data value exceeding one standard deviation from the mean is identified.
3. As an extra precaution, an additional 30 seconds of buffer is added from that point. Everything before this is considered as calm water and clipped away.

4. Starting from the end of the time series and working in reverse, the first data value exceeding one standard deviation from the mean is identified.

5. Similarly, an additional 30 seconds buffer is added from that point. Everything before this is considered calm water and clipped away.

This process is carried out on the time series for Wave gauge 1 (WG1), with all other time series clipped using the same start and end points.




Figure 4.2: Four plots visualizing the different steps of the clipping process of raw data to remove periods of calm water at the start and end of the raw time series.

## 4.2. Wave Propagation on an Empty Foreshore

This section analyses the data from the 3 experiments that were carried out without the artificial reef. The objective was to find out the interaction of the waves with the sloping foreshore and beach without the influence of any structures. The wave gauges were placed along the flume based on the configuration of the Position 1 tests. The positions of the wave gauges for these tests relative to the different reef positions can be seen in Figure 4.3. Note that Wave Gauge 9 was placed on the beach and not on the foreshore.

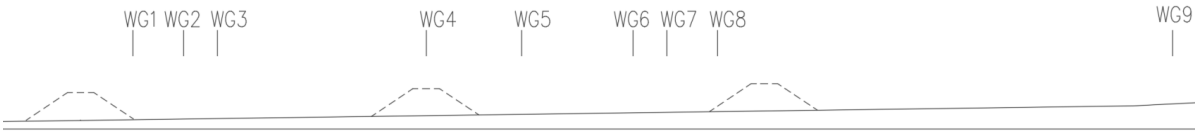



Figure 4.3: Placements of the wave gauges for the tests without the reef relative to the three reef positions

Spectral analysis of the wave signal at each wave gauge was carried out to determine the evolution of the significant wave height and wave period along the foreshore. The results can be seen in Figure 4.4.

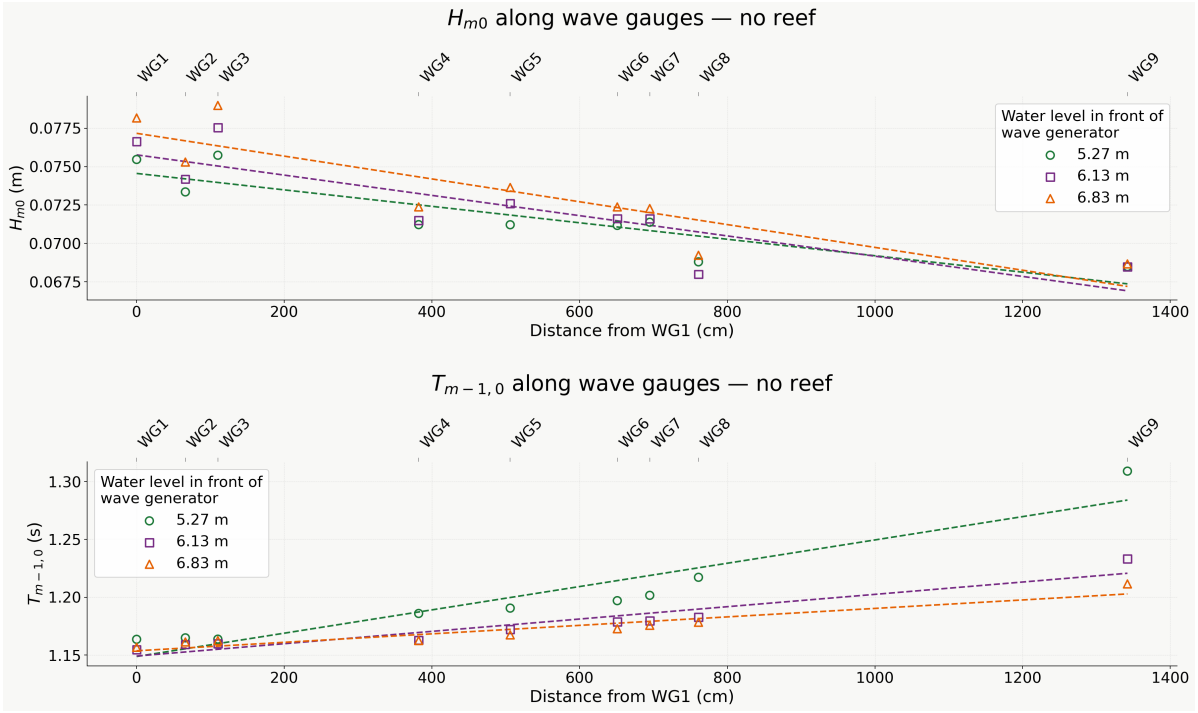



Figure 4.4: Evolution of the significant wave height $H_{m0}$ and spectral period $T_{m-1,0}$ as waves travel along the sloped foreshore in the absence of the artificial reef. The x axis values are the distance of the wave gauges relative to Wave Gauge 1.

As expected we observe that the significant wave height $H_{m0}$ decreases as the wave propagates along the foreshore slope. This overall decrease in wave height and wave energy indicates that mild shoaling effects were outweighed by energy loss due to surface friction with the bottom and the side panels of the flume. Wave breaking along the foreshore slope, that was physically observed in the laboratory, could also explain the loss in wave energy.

Linear regression lines were fitted to the data to investigate and quantify the evolution of the wave characteristics along the foreshore, as shown in Figure 4.4. Based on the regression lines, the value of $H_{m0}$ at Wave Gauge 8 decreased by six to seven percent of its value at Wave Gauge 1. The spectral wave period $T_{m-1,0}$ was also observed to increase, signifying a transformation to longer waves further along the foreshore. The regression lines further showed that the value of $T_{m-1,0}$ at Wave Gauge 8

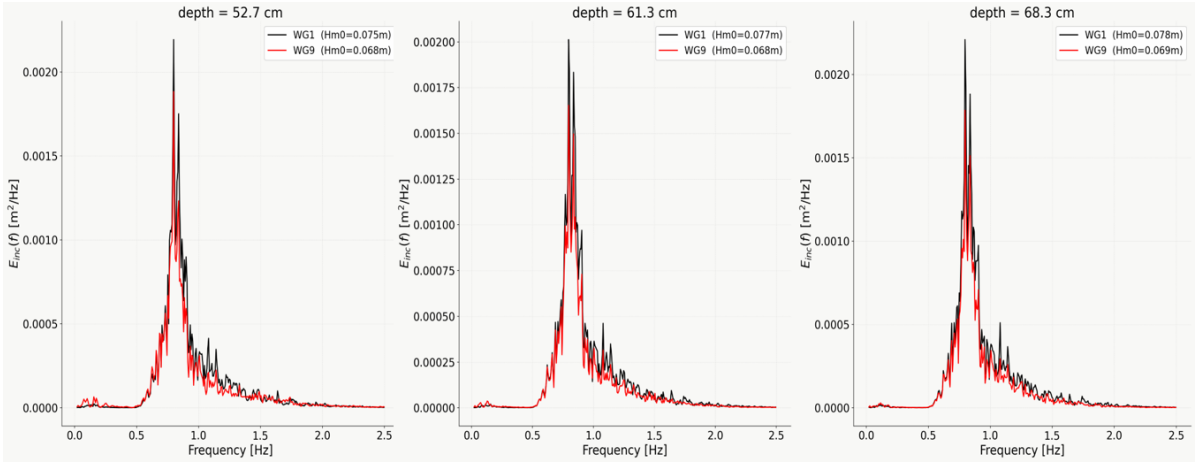



Figure 4.5: Wave energy spectra at Wave Gauge 1 and Wave Gauge 9 for the no-reef tests across three still water depths. The reduction in spectral energy between WG1 and WG9 reflects the natural wave energy dissipation along the flume in the absence of the reef structure.

increased by 2 to 7% of its value at Wave Gauge 1. The decrease in $T_{m-1,0}$ can be explained using Figure 4.5 which shows the difference in the wave energy spectra for WG1 and WG3 for the three tests with an empty foreshore. From WG1 to WG9, a greater dissipation of energy from the higher frequencies was observed. Thus the energy spectra at WG9 has relatively more energy at the lower frequencies leading to a higher $T_{m-1,0}$.

## 4.3. Decomposition of Wave Signal into Incident and Reflected Waves

The wave signal measured by Wave Gauges 1,2 and 3 is a result of the interaction between the incoming and reflected waves. Hence decomposition of the measured wave signal into its incoming and reflected wave components was required. This was carried out using the method of Zelt and Skjelbreia (1993). For the decomposition of the measured wave signal into incident and reflective waves, Wave Gauges 1,2 and 3 were used for the region seaward of the artificial reef and Wave Gauges 6,7,8 were used for the region shoreward of the artificial reef. The decomposition setup is visualized with Figures 4.6 and 4.7.

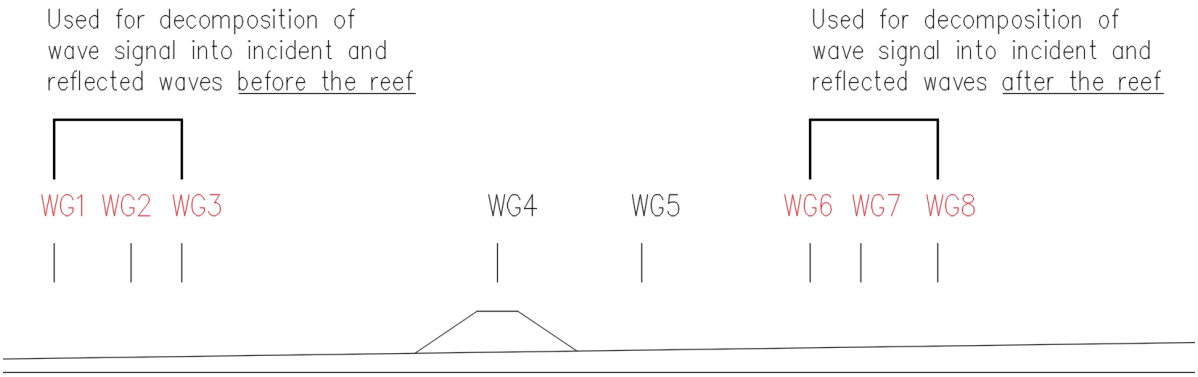



Figure 4.6: Two groups of wave gauges are used to decompose wave signal into incident and reflected waves in regions before and after the reef

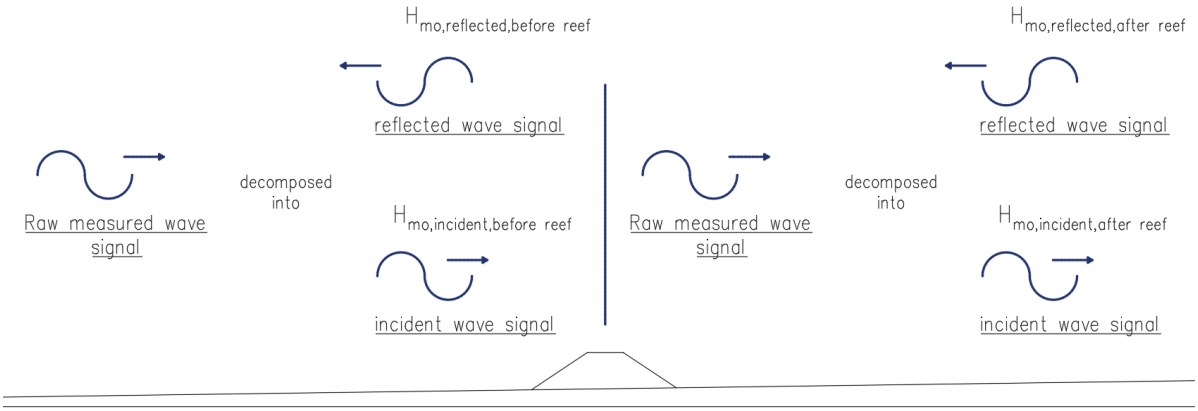



Figure 4.7: Decomposition of raw measured wave signals into constituent reflected and incident wave signals with their respected spectral significant wave heights $H_{m0}$

As seen in figure 4.7, decomposition of the wave signal before the reef produced $H_{m0,reflected,before\ reef}$ and $H_{mo,incident,before\ reef}$ while the decomposition of the wave signal after the reef produced $H_{m0,reflected,after\ reef}$ and $H_{mo,incident,after\ reef}$ . The wave reflection coefficient $K_r$ for before and after the reef can then be calculated as:

$$K_{r,before\ reef} = \frac{H_{m0,reflected}}{H_{mo,incident}} \tag{4.1}$$

### Approximation of seaward incident and reflected wave heights for Position 2

For reference, the relative positions can be seen in Figure 4.8 below.

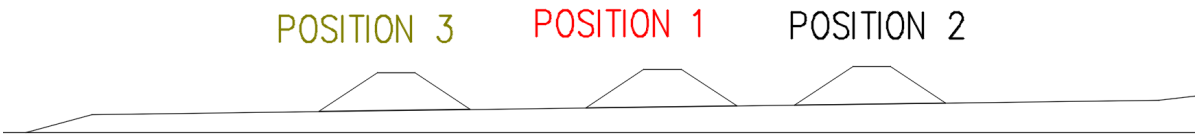



Figure 4.8: Relative positions of the reef for reference

As mentioned earlier in the chapter on Methodology, due to an oversight when marking the positions of the wave gauges along the flume, Wave Gauges 1,2,3 were placed 72 cm closer to the seaward toe of the reef as compared to that for Positions 1 and 3.

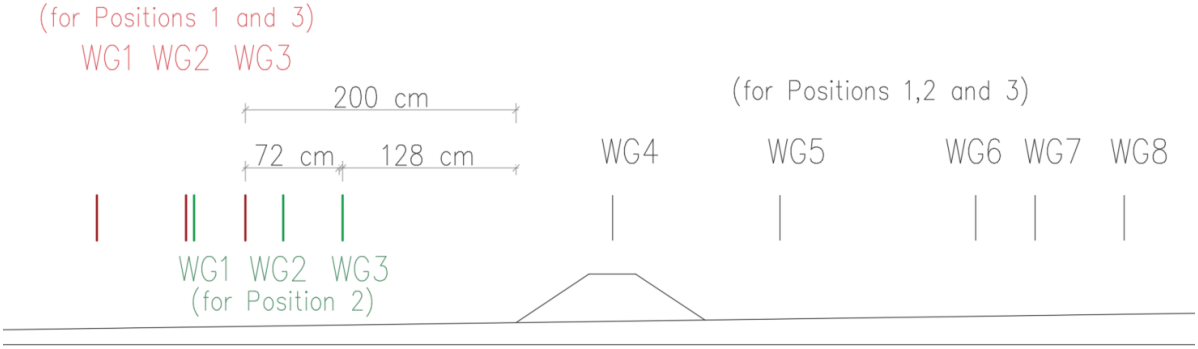



Figure 4.9: Array of Wave Gauges 1,2 and 3 are 72 cm closer to the reef for Position 2 as compared for Positions 1 and 3. The positions of the other wave gauges relative to the reef remain the same

As a result, for Position 2, the distance between Wave Gauges 3 and the seaward toe of the reef was only 128 cm as compared to 200 cm for Positions 1 and 3. Klopman and van der Meer (1999) carried out tests to investigate the changes in the significant wave height and the wave spectrum near a reflective structure. From their findings it was recommended that the distance between the closest wave gauge used for wave decomposition and a structure should be more than $0.4 * L_p$, where $L_p$ is the wave length associated with the local water depth and peak period. It was observed that when this condition was not met, the structure would influence the results of the decomposition leading to elevated values of $K_r$ and dips in the value of $H_{m0,incident}$. Dean and Dalrymple (1991) suggests that this may be due to the influence of evanescent wave modes in the vicinity of the structure. These are non-propagating wave components that decay exponentially with distance from the structure and are therefore only detectable in the near-field region closer to the reef.

Due to the decreased distance between Wave Gauge 3 and the reef, for Position 2, up to 82% of tests violate this condition. The effect of which can then be observed from the analysis of the data from the decomposition of waves before the reef. The effect of the decreased distance can be seen Figures 4.11 and 4.12 where the $H_{m0,incident}$ values for Position 2 are lower and the calculated $K_r$ values are much higher than expected as compared to that for Position 1 and 3. Wave decomposition using only WG1 and WG2 was also attempted for the Position 2 tests, taking advantage of their greater distance from the reef structure. However, the results showed similar signs of compromise and could therefore not serve as a reliable substitute for the three-gauge decomposition method.

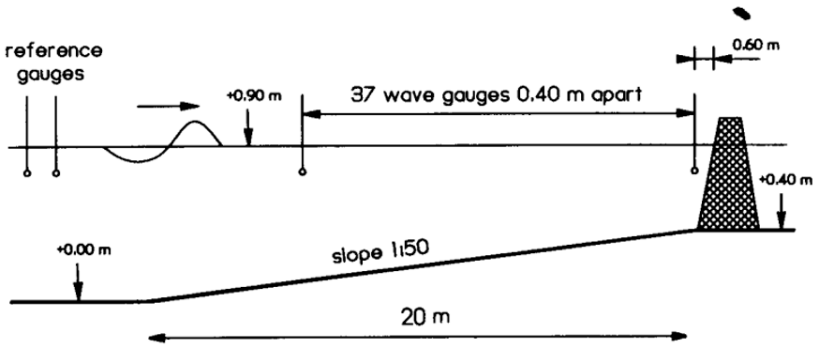



Figure 4.10: Physical model used in the study by Klopman and van der Meer (1999)

Table 4.1: Comparison of test conditions between Klopman and van der Meer (1999) and Position 2 tests

| | Klopman and van der Meer (1999) | Position 2 |
|---|---|---|
| Number of tests | 2 | 33 |
| $H_{m0}$ (m) | 0.206 – 0.209 | 0.120 – 0.200 |
| $s_{m-1,0}$ | – | 0.015 – 0.040 |
| $s_{op}$ | 0.02 – 0.04 | 0.013 – 0.033 |
| $L_p$ (m) | 3.55 – 4.44 | 3.02 – 7.94 |
| Still water depth at toe, $h$ (m) | 0.500 | 0.584 – 0.734 |
| $L_p/h$ | 7.10 – 10.44 | 4.39 – 12.66 |
| Foreshore slope | 1:50 | 1:72.6 |
| Structure slope | 1:1.5 | 1:1.5 |
| Structure type | Permeable rubble mound breakwater | Permeable artificial reef constructed from glued rocks |

The physical model setup used by Klopman and van der Meer (1999) is shown in Figure 4.10. It consisted of a foreshore slope of 1:50 and a rubble mount breakwater with a front slope of 1:1.5 which is the same as the slope of the artificial reef used in this thesis project. A comparison of the test conditions with that of the Position 2 tests can be found in Table 4.1. The considerable overlap in test conditions indicates that the findings from Klopman and van der Meer (1999) can be reasonably applied to the Position 2 tests.

The compromise of the Position 2 test results is further supported by the analysis of the calculated reflection coefficient $K_r$. Figure 4.12 indicates that the $K_r$ values for Position 2 are considerably higher than those of Positions 1 and 3 under matching wave conditions. This is inconsistent with the established empirical expressions for $K_r$, such as Equations 2.4 and 2.5, which indicate that $K_r$ depends on the Iribarren parameter $\xi_p$. Since matching wave conditions and the same reef structure were used across all positions, similar $K_r$ values would be expected. However, the $K_r$ values at Position 2 are approximately twice those of the corresponding Position 1 and 3 tests. This supports the conclusion that the wave decomposition results seaward of the reef at Position 2 have been compromised by the close proximity of WG3 to the toe of the reef structure.

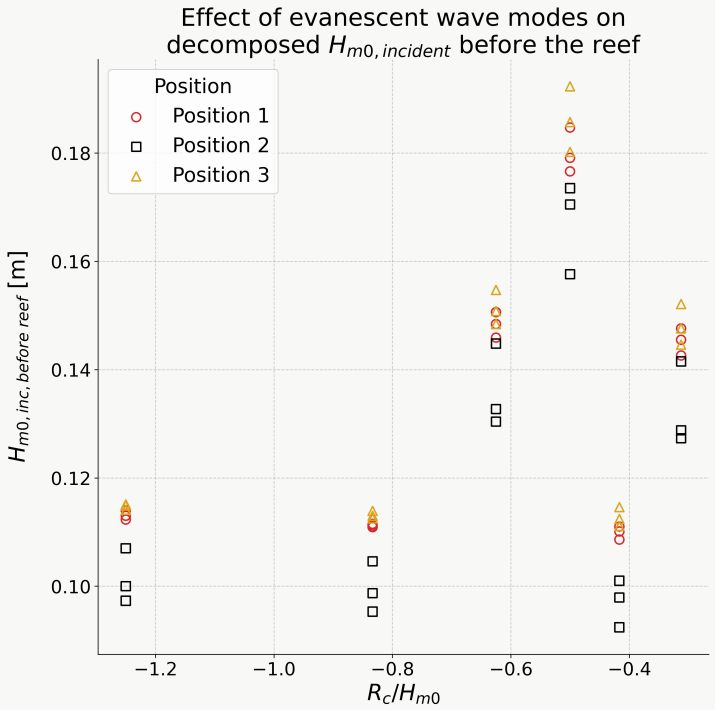



Figure 4.11: Comparison of decomposed incident wave height , $H_{m0,inc}$ before the reef for matched test cases across all three reef positions. Only tests with conditions found in the test plans for all 3 positions were plotted to ensure a fair and clean comparison.

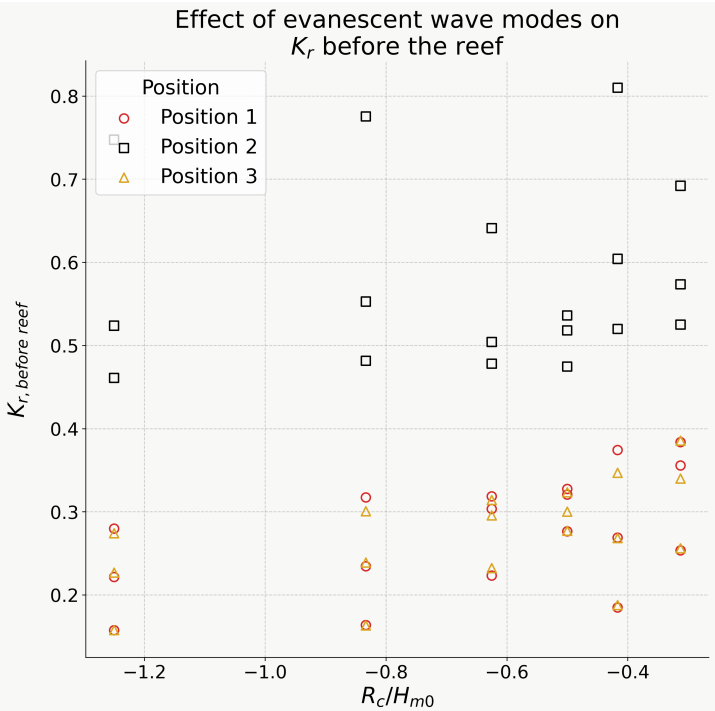



Figure 4.12: Comparison of reflection coefficient, $K_r$, before the reef for matched test cases across all three reef positions. Only tests with conditions found in the test plans for all 3 positions were plotted to ensure a fair and clean comparison.

As a consequence we are unable to confidently make use of results of the decomposition of waves seaward of the reef for the Position 2 tests. The decomposition results for after the reef remains valid for tests from all 3 positions. Subsequent analysis could continue with only using data from Position

1 and Position 3 tests. However this would greatly reduce the range of applicability of the results as the distance between Position 1 and Position 3 is limited to only 4.5 m. So as to not completely omit the data obtained from the Position 2 tests, approximated values for $H_{m0,incident}$ before the reef for Position 2 were generated. This was carried out using the results from the earlier analysis of wave propagation on an empty foreshore. With reference to Figure 4.3 and Figure 4.4, the reef at Position 2 is roughly aligned with that of Wave Gauge 8 from the Position 1 configuration. By accounting for the additional energy dissipation incurred by waves travelling further up the foreshore slope, the incident significant wave height at Position 2 is taken as 6% lower than the corresponding value from Position 3 tests under matching wave conditions (significant wave height, wave steepness and freeboard).

For example, the incident wave height $H_{m0,inc}$ before the reef for a Position 2 test with $H_{m0} = 0.12$ m, wave steepness of $s_{m-1,0} = 0.015$ and freeboard of $R_c = -0.050$ m is approximated as (100-6) times the corresponding incident wave height $H_{m0,inc}$ calculated for Position 3 test with the same wave conditions.

It should be noted that the (100-6)% proportionality constant was derived from the tests with an empty foreshore. Those tests were conducted exclusively with wave conditions of $H_{m0} = 0.08\ m$ and $s_{m-1,0} = 0.040$. The matched Position 2 and Position 3 test pairs, however, involved other wave height values, steepnesses and still water depths. The application of this correction therefore assumes that the (100-6)% proportionality is is not significantly affected by $H_{m0}$, $s_{m-1,0}$ and the still water depth. This is an assumption that could not be independently verified from the available data and represents a source of uncertainty in the corrected Position 2 results.

Out of the 30 tests carried out for Position 2, 11 do not have tests with matching conditions within the test plan of Position 3. The unmatched tests will then be left out of future analyses. Subsequent analyses will make use of data from a reduced number of 115 tests. A plot of the $H_{m0,incident}$ against $R_c/H_{m0}$ with the generated $H_{m0,incident}$ for Position 2 can be seen in Figure 4.13.

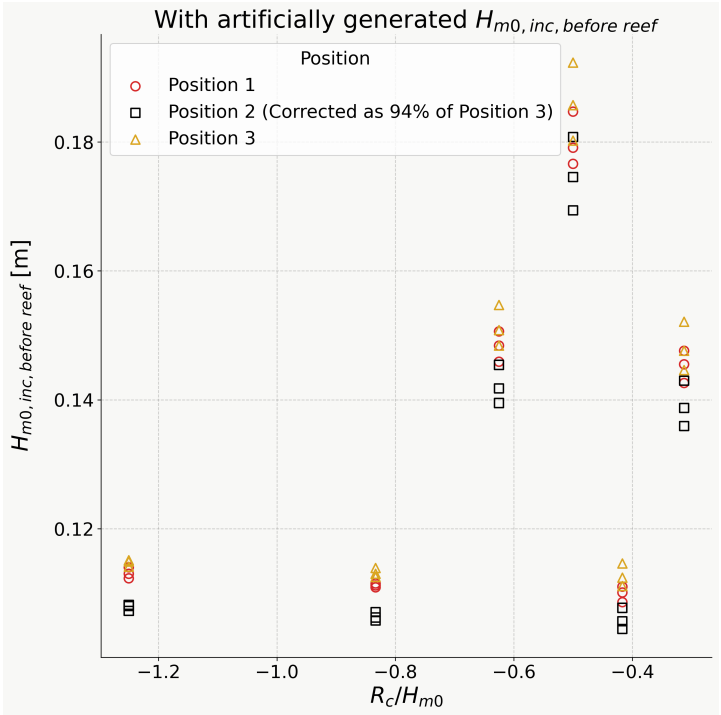



Figure 4.13: Decomposed incident wave height ($H_{m0,inc}$) against $R_c/H_{m0}$ with artificially generated values for Position 2 tests.Only tests with conditions found in the test plans for all 3 positions were plotted

## 4.4. Wave Transmission Analysis

The wave transmission coefficient is defined as the ratio of the transmitted wave height to the incident wave height. The decomposed incident wave before the reef is taken to be $H_{m0,incident}$ and the decomposed incident wave after the reef is taken to be $H_{m0,transmitted}$. The transmission coefficient is hence defined as:

$$K_t = \frac{H_{mo,incident,after\ reef}}{H_{m0,incident,before\ reef}} = \frac{H_{m0,transmitted}}{H_{m0,incident}} \tag{4.2}$$

### 4.4.1. Influence of distance on wave transmission

To investigate the potential influence of distance between the artificial reef and the beach, a plot of $K_t$ against the dimensionless number $R_c/H_{m0}$ was created. The left plot in Figure 4.14 is the measured wave transmission coefficient $K_t$ as function of the relative freeboard $R_c/H_{m0}$ for all test conditions. The right plot shows only the subset of test conditions with overlapping parameters across all three reef positions, providing a fairer comparison by considering only tests conducted under the same wave conditions. A fitted curve is also included in the right plot which illustrates the clear dependency of $K_t$ on $R_c/H_{m0}$.

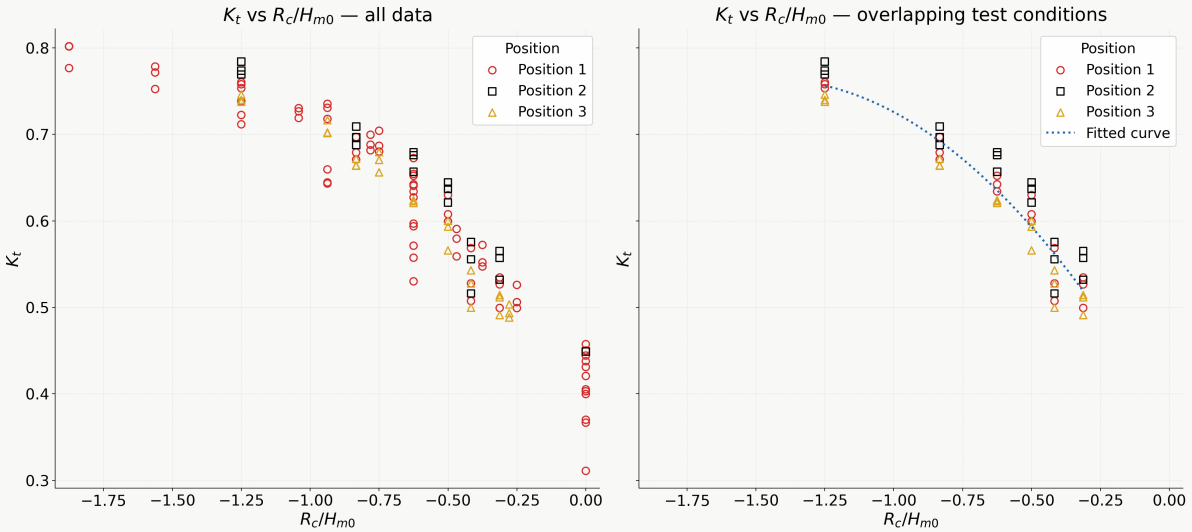



Figure 4.14: Measured wave transmission coefficient $K_t$ as a function of relative freeboard $R_c/H_{m0}$, grouped by reef position. Left: all test conditions. Right: subset of test conditions with overlapping parameters across all three positions, with a fitted curve.

The analysis reveals that the distance between the artificial reef and the beach has a weak influence on the wave transmission coefficient $K_t$. A shorter distance, as represented by Position 2, yields slightly larger $K_t$ values compared to a greater distance, as represented by Position 3. Thus Figure 4.14 indicates that within the tested parameter range, the distance between a permeable low-crested structure and the beach does not have a significant influence on the extent of wave transmission over the structure. The data also clearly reveals a strong dependency of $K_t$ on the $R_c/H_{m0}$. This is indicated by the fitted curve which shows that $K_t$ decreases for $R_c/H_{m0}$ closer to 0. This conclusion is, however, contingent on the approximated $H_{m0,inc}$ values before the reef at Position 2, which constitutes a notable source of uncertainty in the analysis.

Another method of analysing the influence of distance between the structure and the beach on wave transmission is through the use of a total wave reduction coefficient, $K_{total\ reduction}$. This coefficient is defined as the ratio of the significant wave height measured at the beach by Wave Gauge 9 to the target significant wave height produced at the wave generator. The calculation of $K_{total\ reduction}$ is defined by Equation 4.3. This method, although coarser in nature, would make use of known values unlike before where approximated artificial values for significant waves before the reef at Position 2 were used. A plot of $K_{total\ reduction}$ against relative freeboard $R_c/H_{m0}$ can be found in Figure 4.15. The left

plot in Figure 4.15 includes data from all test conditions. The right plot shows only the subset of test conditions with overlapping parameters across all three reef positions, providing a fairer comparison by considering only tests conducted under the same wave conditions. A fitted curve is also included in the right plot which illustrates the clear dependency of $K_{total\ reduction}$ on $R_c/H_{m0}$.

$$K_{total\ reduction} = \frac{H_{m0,WG9}}{H_{m0}} \tag{4.3}$$

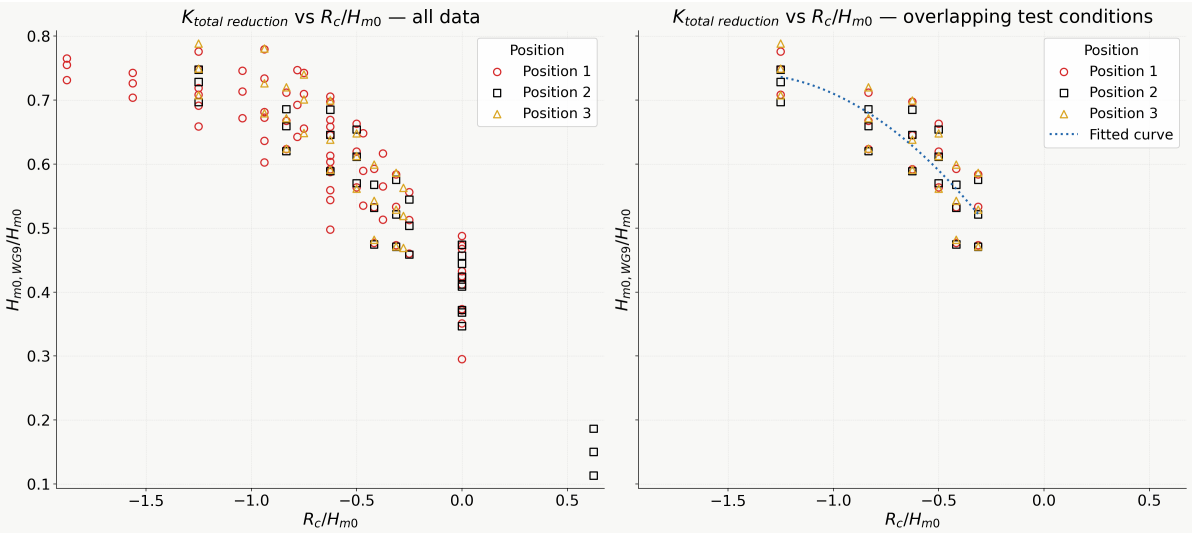



Figure 4.15: The total wave reduction coefficient $K_{total\ reduction}$ is plotted as a function of the relative freeboard $R_c/H_{m0}$ for all test conditions (left). The right plot shows only the subset of test conditions with overlapping parameters across all three reef positions, providing a fairer comparison by considering only tests conducted under the same wave conditions. A fitted curve is also included in the right plot to illustrate the dependency of $K_{total\ reduction}$ on $R_c$.

Similarly, the findings suggests that, within the tested range of parameters that the position of the reef has no significant influence on the total wave reduction from offshore to the beach thus qualitatively supporting our earlier findings from the wave transmission analysis.

### 4.4.2. Influence of wave steepness on wave transmission

The influence of wave steepness $s_{m-1,0}$ on wave transmission was also investigated. Figure 4.16 consists of two plots of $K_t$ against relative freeboard $R_c/H_{m0}$ with the data grouped by wave steepness. The left plot includes data from all test conditions. The right plot shows only the subset of test conditions with overlapping parameters across all three reef positions for a fairer comparison.

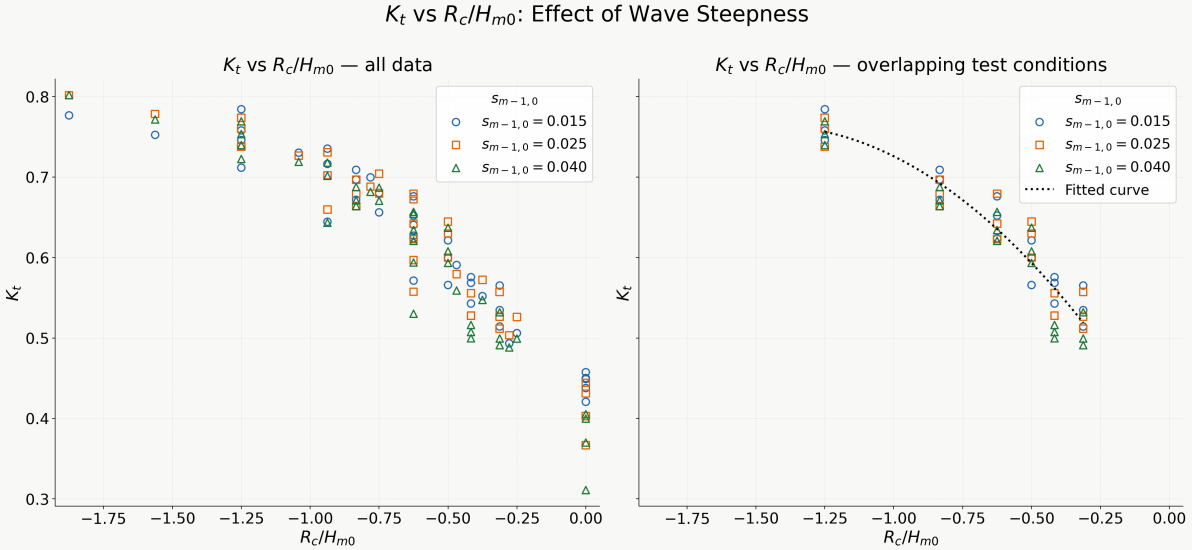



Figure 4.16: The measured wave transmission coefficient $K_t$ is plotted as a function of the relative freeboard $R_c/H_{m0}$ for all test conditions (left). The right plot shows only the subset of test conditions with overlapping parameters across all three reef positions, providing a fairer comparison by considering only tests conducted under the same wave conditions. Both plots are grouped by wave steepness $s_{m-1,0}$, and a fitted curve is included in the right plot to illustrate the overall trend.

Figure 4.16 reveals that, within the tested range of test conditions, for a permeable low-crested structure in front of a nourished beach, the wave steepness has weak influence on the wave transmission coefficient. Although the effect is minor, the analysis indicates that a higher wave steepness would result in a slightly lower $K_t$. This is in line with the results from the tests carried out by Van Gent et al. (2023). Wave steepness primarily influences wave transmission through its effect on wave breaking. For impermeable structures, wave breaking is the dominant dissipation mechanism, resulting in a clear dependence of $K_t$ on wave steepness. For permeable structures, however, energy dissipation through friction and flow through the porous medium becomes comparatively more significant, reducing the relative contribution of wave breaking and consequently diminishing the influence of wave steepness on wave transmission.

### 4.4.3. Influence of other parameters on wave transmission

Other parameters known to influence wave transmission includes the crest width of the structure, the freeboard over the structure, the structure slope and permeability of structure. As the same artificial reef structure was used throughout the entirety of the experiments, the effect of crest width, structure slope and permeability were not investigated. The effect of the freeboard on wave transmission can be seen in Figure 4.14 where wave transmission decreases as the structure becomes less submerged ($R_c$ becomes less negative).

### 4.4.4. Transformation of spectral wave period $T_{m-1,0}$

Changes in the spectral wave period $T_{m-1,0}$ can also be observed for waves which travel over the artificial reef. A plot of the ratio of $T_{m-1,0}$ after and before the reef is seen in Figure 4.17. The value of $T_{m-1,0}$ was obtained from the decomposition of waves before and after the reef. As explained earlier, as the decomposition of waves before the reef for the Position 2 tests were compromised, the transformation of the wave period for Position 2 tests are not analysed here.

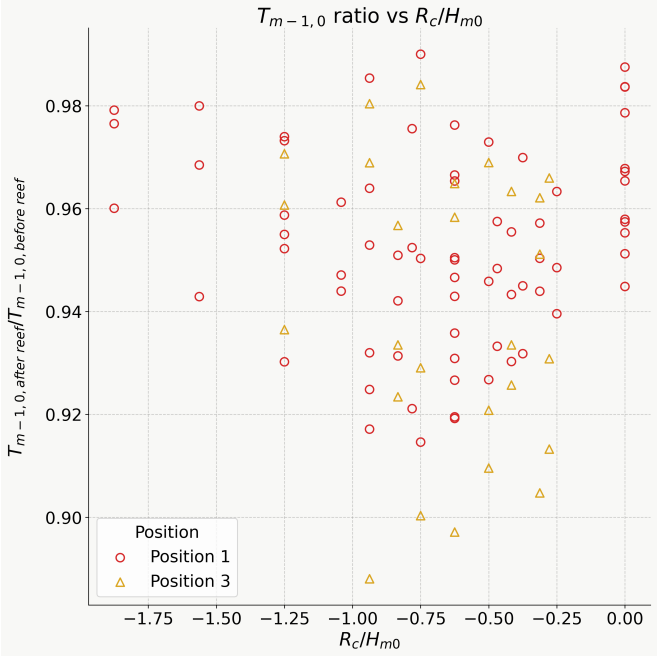



Figure 4.17: Plot of the ratio of $T_{m-1,0}$ after and before the reef

The wave period after the reef was seen to decrease from between 1 to 11% of its value before the reef. The influence of distance between the reef and the beach on the extent of change in wave period is negligible. The decrease in $T_{m-1,0}$ seems to increase for less negative values of $R_c$ (less submerged) although the spread of values also increases. The decrease in wave period can be explained from the analysis of the changes in the spectral shape before and after the reef as seen in Figure 4.18.Interaction with the artificial reef reduces the amount of energy at the peak frequency to a larger extent as compared to that for higher frequencies which leads to a lower $T_{m-1,0}$. The presence of a secondary peak in the wave energy spectrum indicates that higher harmonics were generated before the waves passed over the artificial reef. This is attributed to wave breaking upstream of the structure, which was physically observed during the experiments.

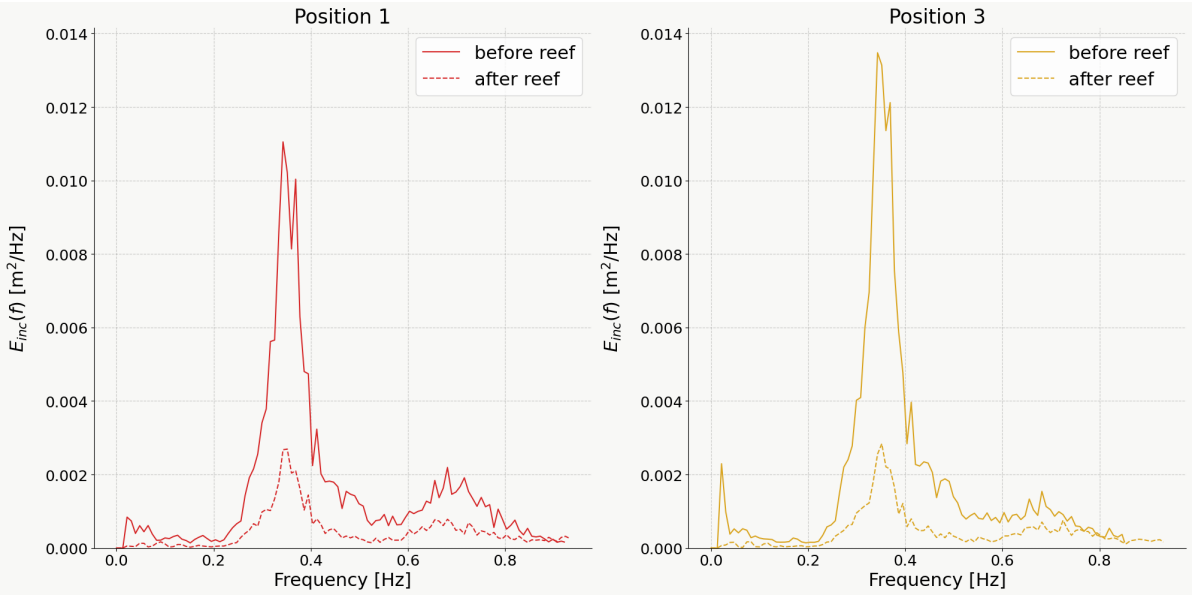



Figure 4.18: Characteristic changes in spectral shape for before and after the reef. Left: Position 1, Right: Position 3

### 4.4.5. Performance of existing empirical formula

The measured $K_t$ were also checked against $K_t$ values calculated using the empirical formula proposed by Van Gent et al. (2023) (see Equation 2.11). This is visualized in Figure 4.19. All of the experiments carried out within this study fall within the ranges of validity for Equation 2.11 which are crest levels between $-2.5 \leq R_c/H_{m0} \leq 2.5$ and crest widths between $0.017 \leq B/L_{m-1,0} \leq 0.27$ (or $0.9 \leq B/H_{m0} \leq 10.6$).

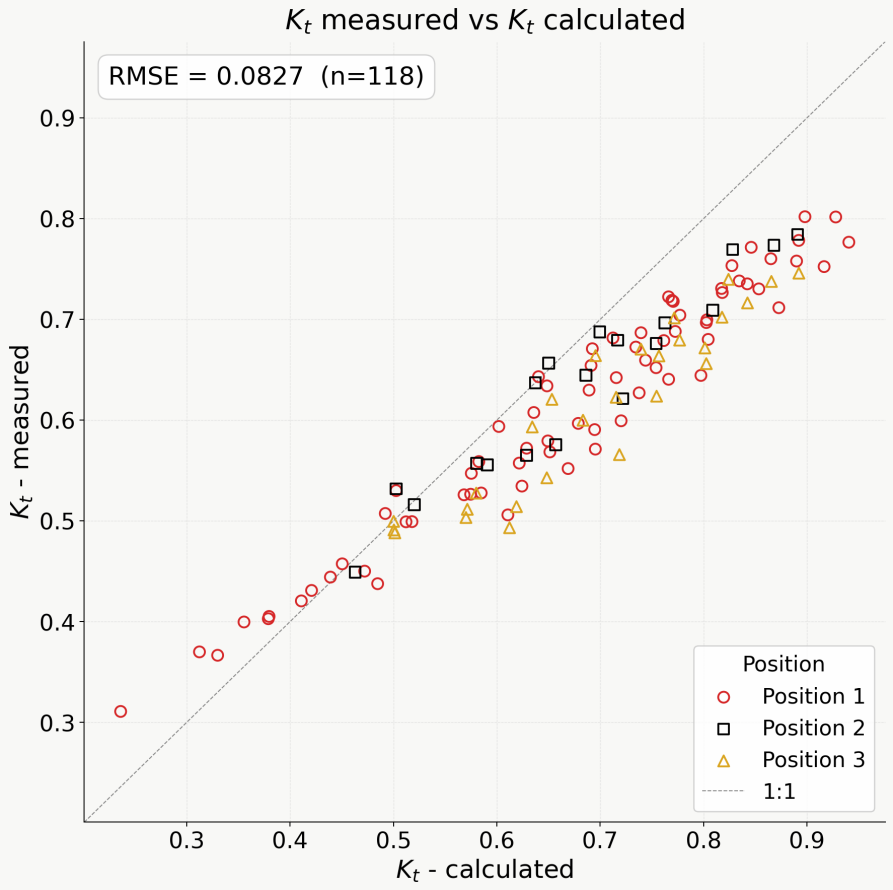



Figure 4.19: Measured versus calculated wave transmission using Equation 2.11. The $R_c/H_{m0}$ value used in the equation has been corrected to factor in the setdown that occurs at the reef.

Equation 2.11 fits data from this project reasonably with an RMSE value of 0.0827. For measured $K_t$ values in the range of 0.2 to 0.6 the equation predicts $K_t$ fairly accurately. For measured $K_t$ values greater than 0.6, there is a visible systemic bias causing the empirical equation to over predict the wave transmission coefficient. A possible reason for the presence of this systemic bias can be explained by the differences between the model setup in the study by Van Gent et al. (2023) and that used in this study. Although the range of wave conditions used were similar, the physical model in this study utilised a sloping foreshore as compared to a horizontal foreshore used by Van Gent et al. (2023) . Over a sloping foreshore, incident waves undergo shoaling and may partially break before reaching the reef, dissipating energy prior to any interaction with the structure. As a result, less wave energy is available for transmission than the formula assumes, leading to a systematic over prediction of $K_t$ by the formula relative to the measured values.

The coefficients c1 and c5 in Equation 2.11 were refitted to address this systemic bias. The refitting of these coefficients reduced the bias by causing a rotation and translation in the scatter plot of Figure 4.19. Coefficient c1 decreased from 0.45 to 0.333 and c5 decreased from 0.50 to 0.487. The new equation now has a reduced RMSE of 0.0296 with the measured wave transmission data. The updated $K_t - measure$ vs $K_t - calculated$ plot is visualized in Figure 4.20.

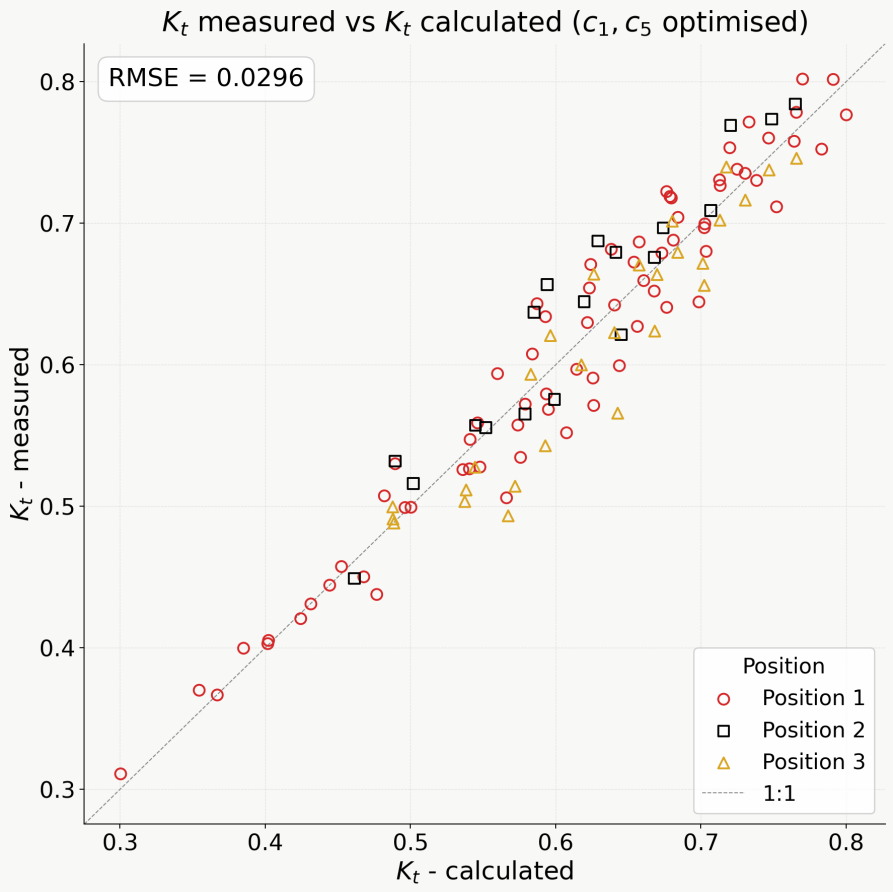



Figure 4.20: Measured wave transmission coefficient $K_t$ plotted against the values calculated using Equation 2.11 with refitted c1 and c5 coefficients. The new coefficient values are $c_1 = 0.333$, $c_5 = 0.488$.

Figure 4.21 presents the optimised transmission formula plotted against the measured $K_t$ values as a function of $R_c/H_{m0}$. The formula curve is evaluated at the mean relative crest width $B/L_{m-1,0}$ across all test conditions, with the shaded region representing the 90% confidence interval of $\pm 0.034$ derived from the standard deviation of the residuals. The general trend of decreasing $K_t$ with increasing submergence depth is well captured by the optimised formula. The scatter about the curve reflects the influence of the remaining free parameters, primarily wave steepness and crest width, which vary across tests but are not represented on this axis. The majority of data points fall within the 90% confidence band, indicating that the optimised formula provides a reasonable prediction of wave transmission for the range of conditions tested.

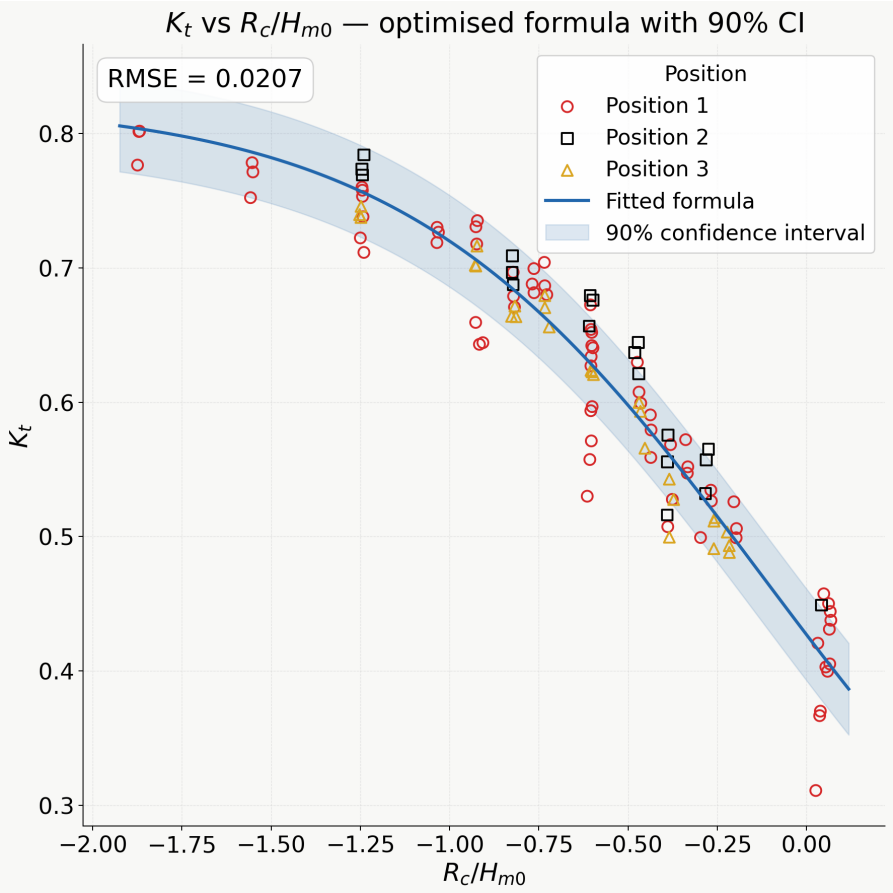



Figure 4.21: Measured wave transmission coefficient $K_t$ plotted against the relative freeboard $R_c/H_{m0}$, with the refitted Van Gent et al. (2023) formula shown as a solid line and the associated 90% confidence interval shown as the shaded region. The formula curve is evaluated at the mean relative crest width $B/L_{m-1,0}$ across all test conditions.

## 4.5. Structure Induced Wave Setup

The structure induced wave setup was determined by calculating the increase in mean water level due to the interaction of the waves with the structure. Each wave gauge was calibrated prior to the experiments to obtain a calibration coefficient in the units of volts/meter, which relates the measured voltage to the water depth at that gauge location. The wave-induced setup,$\delta$, is calculated using equation 4.4 and is visualized in Figure 4.22. The calibration process and calibration coefficients for each wave gauge is found in Appendix A.

$$\delta = \frac{V_{waves} - V_{calm}}{c} \tag{4.4}$$

where:

$V_{calm}$ is the mean voltage in the absence of waves, taken as the mean of the first 5 s of each raw time series

$V_{waves}$ is the mean voltage in the presence of waves, taken as the mean of the clipped time series

$c$ is the calibration coefficient (V/m)

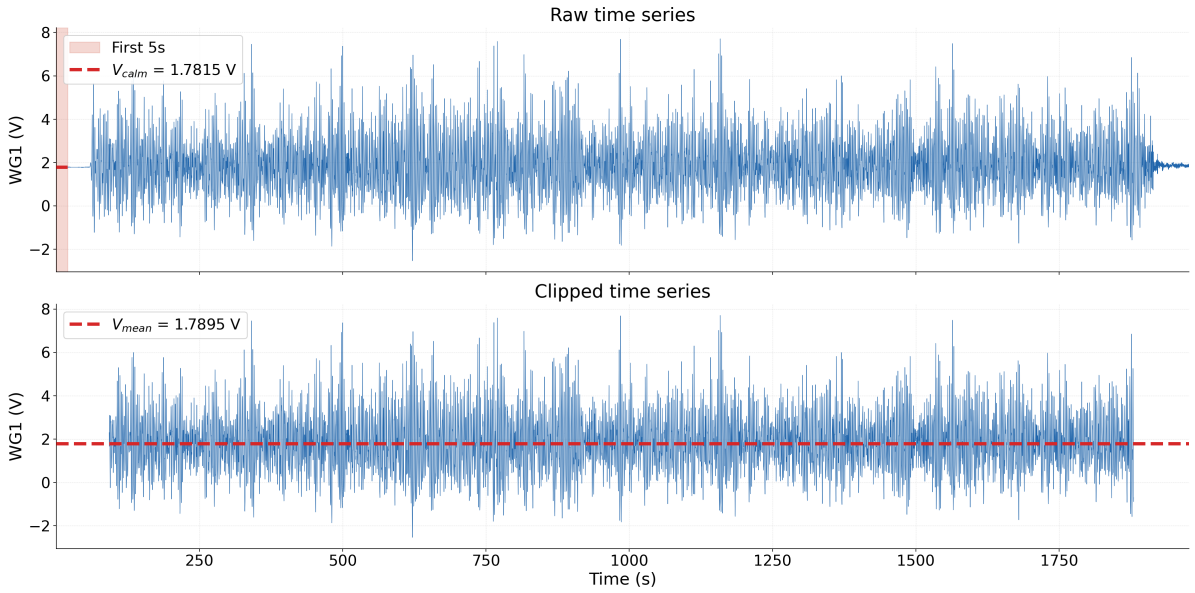



Figure 4.22: Top: Raw time series with calm waters at the start used to determine $V_{calm}$. Bottom: Clipped time series with only waves to determine $V_{mean}$

A set down or decrease in the mean water level seaward of the artificial reef is expected due to the mass balance of water within the flume. Hence the final structure induced wave setup is calculated using Equation 4.5 and visualized in Figure 4.23.

$$\delta_{actual} = \delta_{before\,reef} + \delta_{after\,reef} \tag{4.5}$$

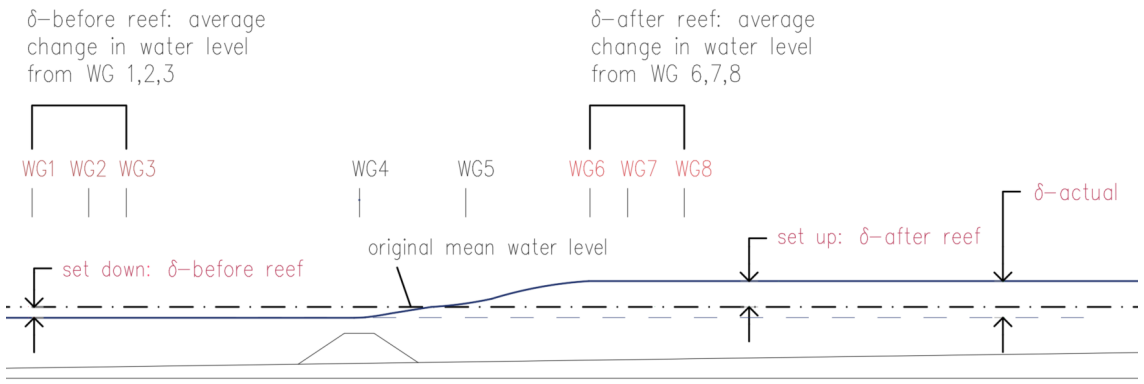



Figure 4.23: Calculation of actual wave setup $\delta_{actual}$ as a sum of observed wave setup after the reef and observed wave setdown before the reef

In subsequent analyses, the freeboard $R_c$ has been adjusted to factor in the setdown at the crest of the artificial reef. The value of this setdown is taken to be the setdown that is calculated at the position of WG3. The corrected freeboard at the crest is determined using Equation 4.6. Where $\delta\ WG3$ is the setdown that occurs at WG3.

$$R_{c,corrected} = R_c - \delta\ WG3 \tag{4.6}$$

### 4.5.1. Influence of distance on structure induced wave setup

From Figure 4.24, the data reveals that within the tested range of parameters, the distance between the artificial reef and the beach has no significant influence over the structure induced wave setup.

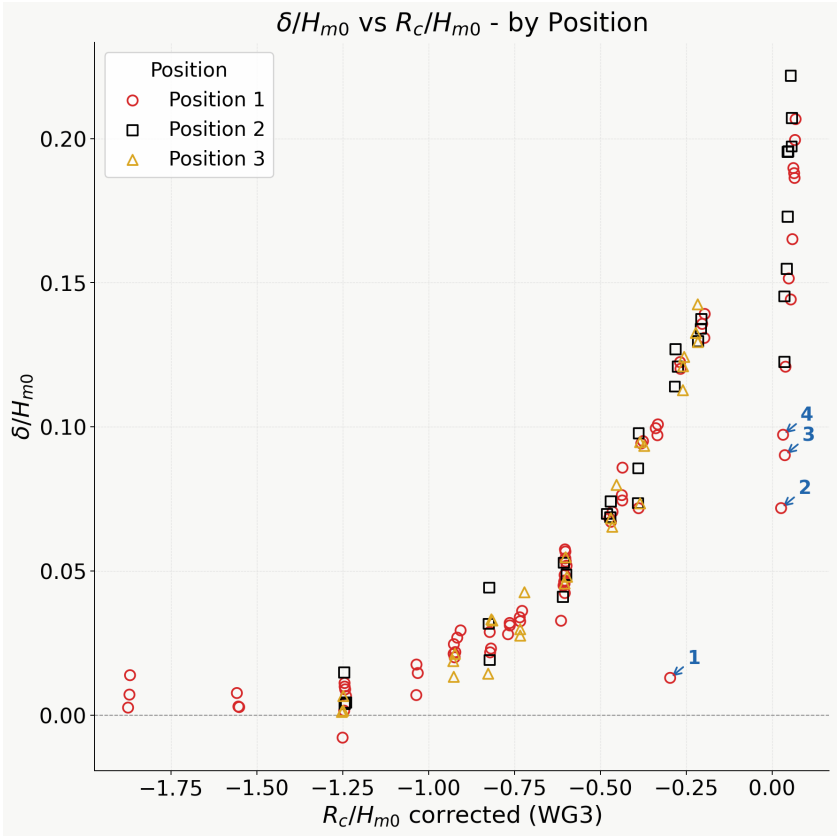



Figure 4.24: Plot of non-dimensional structure induced wave setup $\delta/H_{m0}$ against relative freeboard $R_c/H_{m0}$ grouped by position of reef.$R_c/H_{m0}$ has been corrected to factor in the setdown that occurs at the reef.

Four outlier data points were identified and labelled in Figure 4.24. All of the outliers were from Position 1 tests. Outliers 2,3 and 4 had wave conditions of $H_{m0} = 0.08\ m$, $R_c = 0.000\ m$ and $s_{m-10} = 0.040,\ 0.025\ \&\ 0.015$ respectively. The relatively low incident wave height of $H_{m0} = 0.08$ m may have contributed to the lower than expected wave setup observed for this case. Upon inspection, no faulty measurements were detected in the dataset, and outlier 2 is therefore considered a genuine measurement anomaly. For outlier 2, the averaged water levels recorded at WG6, WG7 and WG8 indicated an overall setdown leeward of the reef rather than the expected setup.

### 4.5.2. Influence of wave steepness on structure induced wave setup

Likewise, from Figure 4.25, it can be seen from the data that, within the range of tested parameters, there is a weak influence of the wave steepness on the extent of the structure induced wave setup. Where a smaller wave steepness results in a slightly larger wave setup.

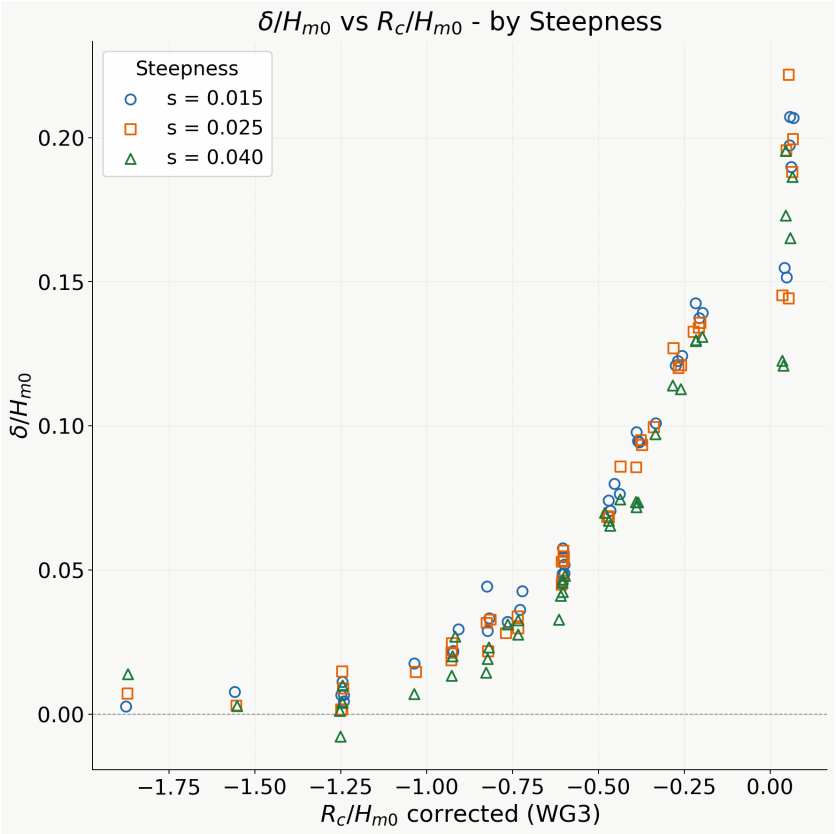



Figure 4.25: Plot of non-dimensional structure induced wave setup $\frac{\delta}{H_{m0}}$ against relative freeboard $\frac{R_c}{H_{m0}}$ grouped by wave steepness.

### 4.5.3. Influence of freeboard on structure induced wave setup

From Figures 4.24 and 4.25, there is a clear dependency on the freeboard over the structure induced wave setup. Less negative values of $R_c/H_{m0}$ , corresponding to less submerged conditions, results in greater structure induced wave setup.

### 4.5.4. Performance of existing empirical formula

Measured setup values were plotted against calculated setup values using the empirical equation proposed by Van Gent (2024) (see Equation 2.14). An RMSE value of 0.0308 was obtained between the measured and calculated values of $\delta/H_{m0}$. The data reveals a systemic bias whereby the empirical formula tends to under predict $\delta/H_{m0}$. This occurs for the range of measured $\delta/H_{m0} > 0.075$. Measured wave setup ranges from a slight setdown of −0.63 mm up to a maximum of 44.4 mm, with a mean of 11.8 mm.

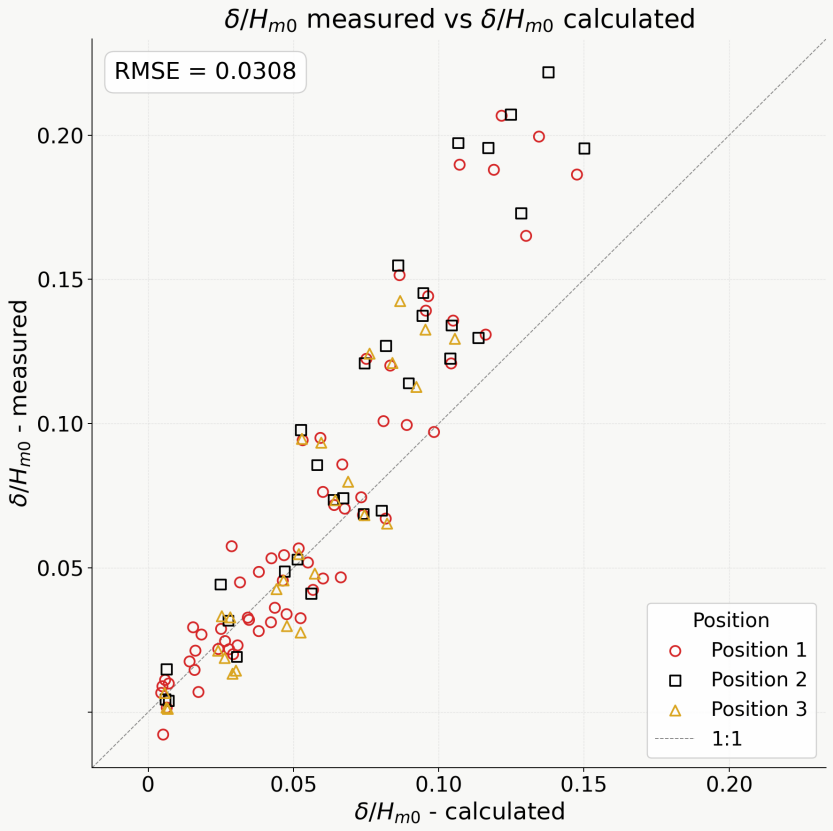



Figure 4.26: Measured setup versus calculated setup based using equation 2.14

Equation 2.14 was fitted using data from tests with experiment conditions parameters within certain ranges. However some of this project's tests were carried out with conditions that fell outside of those ranges. Table 4.2 shows the differences in the range of conditions between those used to fit equation 2.14 and those used for this project.

Table 4.2: Ranges of experiment conditions for those used to fit Equation 2.14 and for this project

| From experiments used to fit Equation 2.14 | From experiments in this project |
|---|---|
| $0.008 \leq s_{m-1,0} \leq 0.040$ | $0.015 \leq s_{m-1,0} \leq 0.040$ |
| $1.5 \leq \frac{h_c}{H_{m0}} \leq 3$ | $1.75 \leq \frac{h_c}{H_{m0}} \leq 4.375$ |
| $-0.8 \leq \frac{R_c}{H_{m0}} \leq 0$ | $-1.875 \leq \frac{R_c}{H_{m0}} \leq 0.625$ |
| $0.94 \leq \frac{B}{H_{m0}} \leq 2.35$ | $1.75 \leq \frac{B}{H_{m0}} \leq 4.375$ |
| $0.19 \leq \frac{D_{n50}}{H_{m0}} \leq 0.47$ | $0.2 \leq \frac{D_{n50}}{H_{m0}} \leq 0.5$ |

Figure 4.27 shows two plots of measured versus calculated $\delta/H_{m0}$. The left plot is for tests with condition values which fall within the valid range of Equation 2.14. Excluding the data points from tests with conditions that fall outside of the valid range results in an RMSE value of 0.0372. From among the 129 tests that was carried out, 68 tests were valid, 51 tests had conditions outside the valid range and 10 tests could not produce a calculated $\delta/H_{m0}$ as those had negative $(\delta/H_{m0} + 1.5)$ values which when raised to the power of 1.5 in Equation 2.14 led to a mathematical error. For the points outside the valid range, an RMSE value of 0.0193 was obtained. This indicates that Equation 2.14 performs reliably even for tests with conditions outside of its valid range.

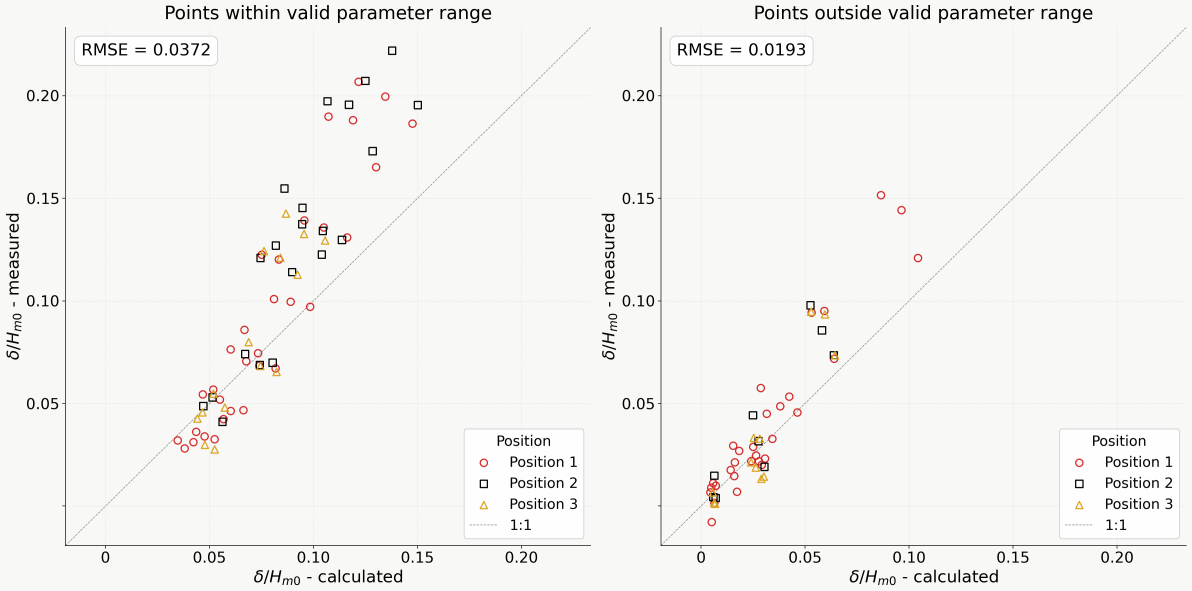



Figure 4.27: Measured vs. calculated $\delta/H_{m0}$ for tests within (left) and outside (right) the valid range of Equation 2.14.

To address the systemic bias present in the current formulation. The coefficients of Equation 2.14 were refitted. Increasing the 0.22 to 0.2887 in Equation 2.14 resulted a rotation of the scatterplot in Figure 4.26 and an improved RMSE value of 0.0216. The new $\delta/H_{m0} - measured$ vs $\delta/H_{m0} - calculated$ plot can be see in Figure 4.28

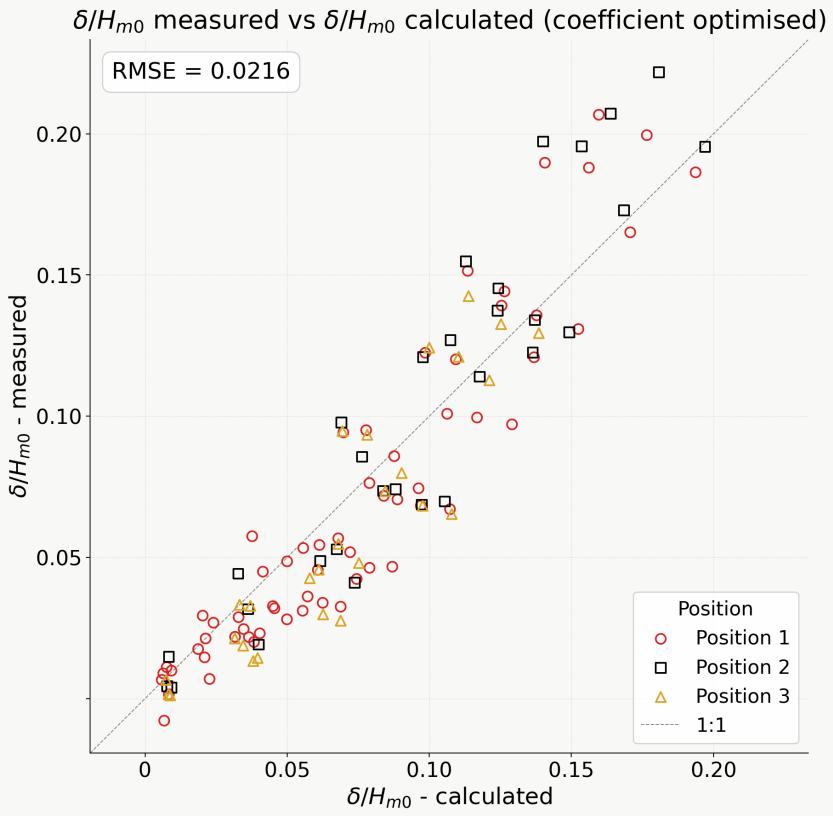



Figure 4.28: Measured wave setup $\delta/H_{m0}$ plotted against the values calculated using the empirical setup formula with the leading coefficient refitted from 0.22 to 0.289, grouped by reef position.

Figure 4.27 was replotted with the refitted formula as Figure 4.29. The RMSE for the data points with the range of validity improved to 0.0258 and the RMSE of the data points outside of the range of validity improved to 0.0140.

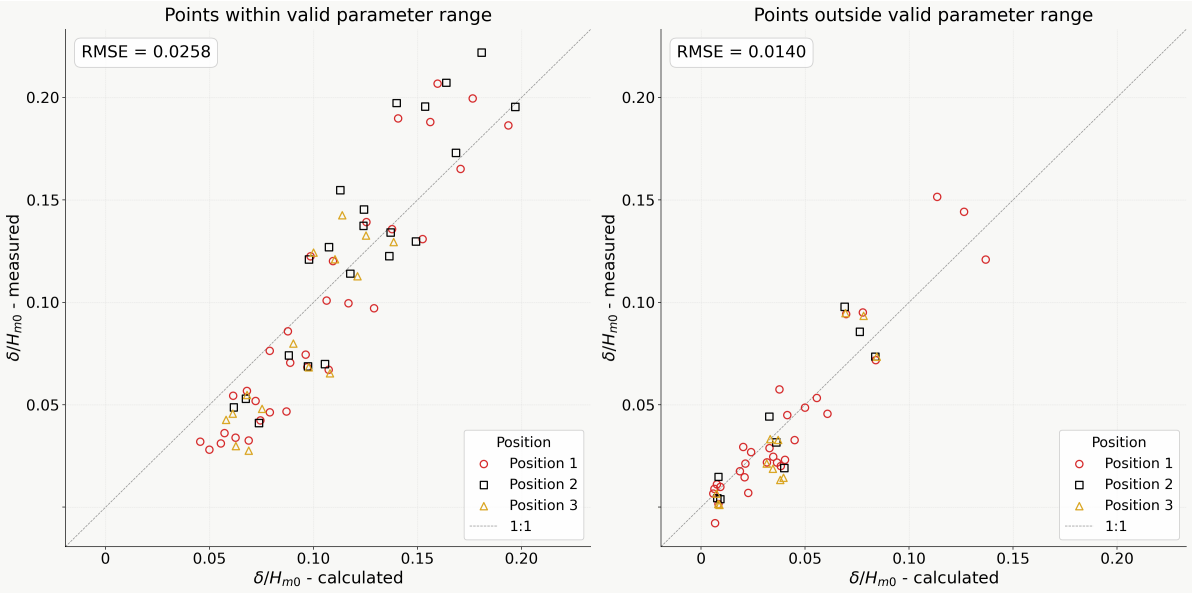



Figure 4.29: Measured vs. calculated $\delta/H_{m0}$ for tests within (left) and outside (right) the valid range of Equation 2.14.

Figure 4.30 presents the optimised setup formula plotted against the measured $\delta/H_{m0}$ values as a function of $R_c/H_{m0}$. The formula curve is evaluated at the mean wave steepness $s_{m-1,0}$ and mean

relative crest height $h_c/H_{m0}$ across all test conditions, with the shaded region representing the 90% confidence interval of $\pm 0.035$ derived from the standard deviation of the residuals. The general trend of increasing wave setup with decreasing submergence depth is well captured by the optimised formula. The scatter about the curve reflects the influence of the remaining parameters, primarily wave steepness and relative crest height, which vary across tests but are not represented on this axis. The majority of data points fall within the 90% confidence band, indicating that the optimised formula provides a reasonable prediction of wave setup for the range of conditions tested.

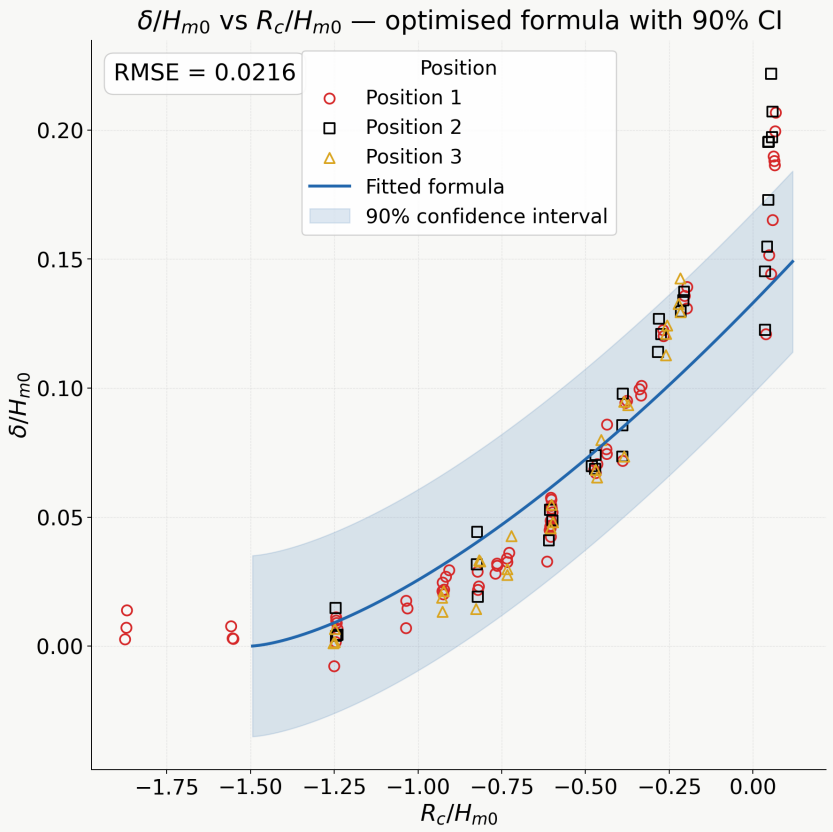



Figure 4.30: Measured wave setup $\delta/H_{m0}$ plotted against the relative freeboard $R_c/H_{m0}$, with the optimised setup formula shown as a solid line and the associated 90% confidence interval shown as the shaded region. The formula curve is evaluated at the mean wave steepness $s_{m-1,0}$ and mean relative crest height $h_c/H_{m0}$ across all test conditions.

# 5

# Discussion

## 5.1. Research Limitations and Sources of Uncertainty

The sources of uncertainty in this project may originate from human error whilst carrying out the physical model experiments, faulty measuring equipment and also from the different schematization mentioned beforehand. Human error can be minimized and contained through proper planning and careful execution of the physical model tests and analysis of data. This requires in depth and accurate understanding of the objective of the tasks that are to be carried out. Errors arising from faulty equipment can also be reduced by active monitoring and checking of measured data to look for signs of mis-measurements. Proper handling of sensitive equipment is also essential to preserve its functionality.

A mistake in the model setup resulted in Wave Gauge 3 being positioned only 128 cm from the seaward toe of the reef for Position 2, compromising the wave decomposition results and necessitating approximations for $H_{m0,inc,before\ reef}$. These approximations relied on earlier analysis of wave propagation over an empty foreshore and were based on assumptions that were not fully verified, most notably that the decay in $H_{m0}$ along the foreshore is independent of the significant wave height, wave steepness, and water depth, introducing uncertainty into the subsequently calculated $K_t$ values. Deriving conclusions based solely on Positions 1 and 3 would avoid this source of uncertainty, but limits applicability given the relatively small variation in distance between those two positions. Including the approximated Position 2 values expands the range of variation in reef-to-shore distance, but at the cost of reduced robustness in the derived conclusions.

Limitations of this study arises from the different schematization that were made. For instance, the effect of erosion and scour that occur in reality are not taken into consideration in the physical model. All of the physical model elements from the foreshore slope, the beach slope and reef are of fixed dimensions and are unable to model the dynamic reshaping that occurs in reality due to sediment transport processes. The foreshore and beach were modelled with a wooden impermeable slope while the artificial reef structure in this study was a prismatic trapezoid constructed out of glued rocks. Artificial reefs in reality come in a variety of shapes and materials and may lead to interactions with waves that deviate from the findings of this study. However the findings of the project still retains merit as it provides a baseline for future research with its limitations clearly scoped.

## 5.2. Discussion on Wave Transmission and Structure Induced Wave Setup

The primary conclusion of the wave transmission and structure induced wave setup analysis is that, within the tested experiment conditions, the distance between a low crested permeable structure and a impermeable beach has no significant influence on both phenomena. Wave steepness was also seen to have a limited effect. However there is a clear dependency on the freeboard which proves to be a dominating factor in determining the extent of the wave transmission that occurs over and through the submerged structure. The study however does not investigate the influence of the permeability of the

structure as the same artificial reef was used throughout all the experiments.

The observed decrease in the spectral wave period $T_{m-1,0}$ by waves that travel over and through the artificial reefs and the subsequently analysis of the change in spectral shape of the waves before and after the reef informs us that submerged low crested structures effectively removes energy from relatively lower frequencies. The corresponding longer waves are more dissipated as they have larger orbital velocities that extend deeper into the water column and thus interact more with the structure. This would be useful in the prevention of coastal erosion as long waves are known to be a driving force that transports sediments from the beach away in erosion processes.

## 5.3. Implication on the Implementation of Artificial Reefs

The objective of this physical model study was to better understand the hydrodynamic interaction between waves and artificial reefs for future implementations. Artificial reefs, functioning as offshore submerged breakwaters, is a nature based solution that is attracting increasing interest, especially as a supplementary coastal measure for nourished beaches. Artificial reefs may help to trap sediment, attenuate wave energy, reduce alongshore currents and diminished erosion rates at the nourished beaches. This would reap economic benefits as the period of time between nourishments would be prolonged and the total volume required for the nourishment would be reduced. Locations which have limited access to sediments would greatly benefit from this effect.

Within the tested range of conditions of the study, the data analysis points to the notion that the distance between the artificial reef and a nourished beach does not have a significant influence on wave transmission over the reef. Nor does it significantly influence the structure-induced wave setup that occurs between the reef and the beach. This means that designers of artificial reefs need not place significant consideration on the extra parameter of distance to the beach when determining a suitable location for construction. One implication would be on the economics of the artificial reef construction. If distance to the shore is not a significant factor to be considered, designers may choose sites closer to the shore in shallower waters. In which less material is required to obtain desired freeboard values thus reducing material costs. However other considerations such as construction and maintenance costs will still be primary factors in the economics of artificial reef design.

Rather than fixating on the distance from the shore, designers should focus on the local conditions at the location of interest. This includes parameters such as the local freeboard and the wave climate. It has been proven that failure to determine suitability of a site for artificial reef construction has been a frequent cause for unsuccessful projects. Other key considerations would be the geometric design and material used to construct the reef. These factors affect the permeability of the structure and hence its effectiveness in attenuating wave energy. In short, the findings of this study would allow designers to place more focus on parameters which are known to make a difference on the effectiveness of artificial reefs.

# 6

# Conclusions and Recommendations

## 6.1. Conclusions

Physical model experiments were carried out in a flume to investigate the behaviour of waves travelling over artificial reefs in front of an impermeable beach. The combined use of a permeable low crested structure with the distance between the structure and the beach as a variable, to study wave transmission and structure-induced wave setup, represents a configuration which has not been clearly addressed in existing literature. This study has thus provided novel insights into this area. The range of validity for the results from this study is given as $-1.875 \leq R_c/H_{m0} \leq 0.625$ with $0.015 \leq s_{m-1,0} \leq 0.040$.

### 6.1.1. Wave transmission:

The following conclusions are conditioned on the physical model setup and the range of parameters used in the experiments.

- The distance between a submerged low crested structure (artificial reef) and an impermeable sloped beach has no significant influence on the wave transmission that occurs over the structure.
- Wave steepness has a weak influence on the wave transmission that occurs over permeable low crested structures.
- The spectral wave period $T_{m-1,0}$ decreases for waves that travel over or through a permeable low crested structure.
- Existing empirical formula for wave transmission fits the measured data from this project reasonably well.

### 6.1.2. Structure induced wave setup:

The following conclusions are conditioned on the physical model setup and the range of parameters used in the experiments.

- The distance between a submerged low crested structure (artificial reef) and an impermeable sloped beach has no significant influence on the structure induced wave setup between the structure and an impermeable sloped beach.
- Wave steepness has a weak influence on the structure induced wave setup that occurs between permeable low crested structure and an impermeable sloped beach.
- Existing empirical formula for structure induced wave setup fits the measured data from this project reasonably well.

## 6.2. Recommendations

### 6.2.1. Possible areas for future research

Future studies should focus on the design of artificial reefs which can excel in both its functions as structures to enhance marine life and biodiversity and as submerged breakwaters capable of effectively dissipating wave energy. Current designs of artificial reefs comes in many shapes and materials but are unable to perform both functions to a high degree. Studies should also focus on sustainable construction of artificial reefs which would able to withstand the harsh wave climates and high current velocities. To address the limitations of this study, future research could also make use of structures which are able to have some damage to better model reality. Physical modelling tests involving novel artificial reef designs could also be carried out whilst keeping the distance between the reef structure and the beach as a variable. Greater confidence could thereby be obtained regarding the actual influence of this distance on hydrodynamic processes such as wave transmission and structure-induced wave setup.

### 6.2.2. Physical modelling experiments

Physical modelling experiments represent a significant undertaking, requiring knowledge across a wide array of topics throughout the different phases of a research project. The process is time-consuming, and the repetitive nature of experimental work over prolonged periods creates numerous opportunities for human error. A thorough understanding of the equipment being used, including its capabilities and limitations, is essential, as is careful consideration of the physical model setup, the placement of wave gauges and instrumentation, and the configuration of the data acquisition system. Improper wiring or incorrect identification of measurement channels can lead to erroneous or missing data, the consequences of which may only become apparent during post-processing.

Effective management of complexity is critical to the success of such studies. Breaking larger tasks down into smaller, more manageable components and addressing them systematically reduces the likelihood of oversight. Similarly, unfamiliar concepts and instrumentation can be approached incrementally, building foundational understanding before integrating individual components into a broader framework. Collaboration with experienced supervisors, laboratory technicians, and peers is strongly recommended, as their guidance can significantly reduce the time required to resolve technical challenges and improve the overall quality of the experimental work.

# Bibliography


Allsop, W., & Channell, A. (1989). Wave reflections in harbours: Reflection performance of rock armoured slopes in random waves.

Armono, H., & Hall, K. (2003). Wave transmission on submerged breakwaters made of hollow hemispherical shape artificial reefs. *Canadian coastal conference*, 313–322.

Baine, M. (2001). Artificial reefs: A review of their design, application, management and performance. *Ocean & Coastal Management*, *44*(3-4), 241–259.

Bohnsack, J. A., & Sutherland, D. L. (1985). Artificial reef research: A review with recommendations for future priorities. *Bulletin of marine science*, *37*(1), 11–39.

Bosboom, J., & Stive, M. J. (2021). *Coastal dynamics*. Delft University of Technology.

Briganti, R., van der Meer, J., Buccino, M., & Calabrese, M. (2003). Wave transmission behind low-crested structures. In *Coastal structures 2003* (pp. 580–592).

Calabrese, M., Vicinanza, D., & Buccino, M. (2003). Large-scale experiments on the behaviour of low crested and submerged breakwaters in presence of broken waves. In *Coastal engineering 2002: Solving coastal conundrums* (pp. 1900–1912). World Scientific.

Chiaia, G., Damiani, L., & Petrillo, A. (1992). Evolution of a beach with and without a submerged breakwater: Experimental investigation. In *Coastal engineering 1992* (pp. 1959–1972).

Church, J. A., Clark, P. U., Cazenave, A., Gregory, J. M., Jevrejeva, S., Levermann, A., Merrifield, M. A., Milne, G. A., Nerem, R. S., Nunn, P. D., et al. (2013). *Sea level change* (tech. rep.). PM Cambridge University Press.

Cid, A., Menéndez, M., Castanedo, S., Abascal, A. J., Méndez, F. J., & Medina, R. (2016). Long-term changes in the frequency, intensity and duration of extreme storm surge events in southern europe. *Climate Dynamics*, *46*(5), 1503–1516.

CIRIA, CUR, & CETMEF. (2007). *The rock manual: The use of rock in hydraulic engineering* (2nd ed.).

Clark, J. R. (2018). *Coastal zone management handbook*. CRC press.

Cox, J., & Clark, G. (1992). Design development of a tandem breakwater system for hammond indiana. *Coastal structures and breakwaters: Proceedings of the conference organized by the Institution of Civil Engineers, and held in London on 6&8 November 1991*, 111–121.

da Silva, G. V., Hamilton, D., Strauss, D., Murray, T., & Tomlinson, R. (2022). Sediment pathways and morphodynamic response to a multi-purpose artificial reef–new insights. *Coastal Engineering*, *171*, 104027.

Daemen, I. (1991). Wave transmission at low crested structures; delft hydraulics report h 462. *Delft University of Technology: Delft, The Netherlands*.

d'Angremond, K., Van Der Meer, J. W., & De Jong, R. J. (1996). Wave transmission at low-crested structures. In *Coastal engineering 1996* (pp. 2418–2427).

Dean, R. G. (2003). *Beach nourishment: Theory and practice* (Vol. 18). World scientific publishing company.

Dean, R. G., & Dalrymple, R. A. (1991). *Water wave mechanics for engineers and scientists* (Vol. 2). world scientific publishing company.

Dekker, J., Caires, S., & Van Gent, M. R. A. (2007). Reflection of non-standard wave energy spectra by sloping structures. *Proc. Coastal Structures 2007*, 760–770.

Dinu, I., Gràcia, V., García-León, M., Lin-Ye, J., Stănică, A., & Sánchez-Arcilla, A. (2025). Feasibility of artificial reefs as coastal protection measures at the danube delta coast, romania. *Frontiers in Environmental Science*, *13*, 1568364.

Diskin, M. H., Vajda, M. L., & Amir, I. (1970). Piling-up behind low and submerged permeable breakwaters. *Journal of the Waterways, Harbors and Coastal Engineering Division*, *96*(2), 359–372.

Gallop, S., Bosserelle, C., Pattiaratchi, C., & Eliot, I. (2011). Form and function of natural and engineered perched beaches. *Coasts and Ports 2011: Diverse and Developing: Proceedings of the 20th Australasian Coastal and Ocean Engineering Conference and the 13th Australasian Port and Harbour Conference*, 232–237.

Greenslade, D., Hemer, M., Babanin, A., Lowe, R., Turner, I., Power, H., Young, I., Ierodiaconou, D., Hibbert, G., Williams, G., et al. (2020). 15 priorities for wind-waves research: An australian perspective. *Bulletin of the American Meteorological Society*, *101*(4), E446–E461.

Hamlington, B., Bellas-Manley, A., Willis, J., Fournier, S., Vinogradova, N., Nerem, R., Piecuch, C., Thompson, P., & Kopp, R. (2024). The rate of global sea level rise doubled during the past three decades. *Communications Earth & Environment*, *5*(1), 601.

Hanson, H., Brampton, A., Capobianco, M., Dette, H. H., Hamm, L., Laustrup, C., Lechuga, A., & Spanhoff, R. (2002). Beach nourishment projects, practices, and objectives—a european overview. *Coastal engineering*, *47*(2), 81–111.

Harris, L. E. (2009). Artificial reefs for ecosystem restoration and coastal erosion protection with aquaculture and recreational amenities. *Reef Journal*, *1*(1), 235–246.

Hemer, M. A., Fan, Y., Mori, N., Semedo, A., & Wang, X. L. (2013). Projected changes in wave climate from a multi-model ensemble. *Nature climate change*, *3*(5), 471–476.

Hoffman, E. (2016). The costs of shoreline stabilization [South Atlantic Alliance].

Huang, J., Lowe, R. J., Ghisalberti, M., & Hansen, J. E. (2024). Wave transformation across impermeable and porous artificial reefs. *Coastal Engineering*, *189*, 104488.

Klopman, G., & van der Meer, J. W. (1999). Random wave measurements in front of reflective structures. *Journal of waterway, port, coastal, and ocean engineering*, *125*(1), 39–45.

Leatherman, S. P. (1996). Shoreline stabilization approaches in response to sea level rise: U.S. experience and implications for pacific island and Asian nations. In L. Erda, W. C. Bolhofer, S. Huq, S. Lenhart, S. K. Mukherjee, J. B. Smith, & J. Wisniewski (Eds.), *Climate change vulnerability and adaptation in asia and the pacific* (pp. 149–157). Springer.

Lokesha, Sundar, V., & Sannasiraj, S. (2013). Artificial reefs: A review. *The International Journal of Ocean and Climate Systems*, *4*(2), 117–124.

Longuet-Higgins, M. S. (1967). On the wave-induced difference in mean sea level between the two sides of a submerged breakwater.

Loveless, J., Debski, D., & MacLeod, A. (1999). Sea level set-up behind detached breakwaters. In *Coastal engineering 1998* (pp. 1665–1678).

Nicholls, R. J., & Cazenave, A. (2010). Sea-level rise and its impact on coastal zones. *science*, *328*(5985), 1517–1520.

O'Leary, E., Hubbard, T., & O'Leary, D. (2001). Artificial reefs feasibility study.

Parkinson, R. W., & Ogurcak, D. E. (2018). Beach nourishment is not a sustainable strategy to mitigate climate change. *Estuarine, Coastal and Shelf Science*, *212*, 203–209.

Pilarczyk, K. W. (2003). Design of low-crested (submerged) structures – an overview. *Proceedings of the 6th International Conference on Coastal and Port Engineering in Developing Countries (COPEDEC)*, 1–19.

Pilarczyk, K. W., & Zeidler, R. B. (1996). *Offshore breakwaters and shore evolution control*. CRC Press.

Postma, G. (1989). Wave reflection from rock slopes under random wave attack. *MS thesis, Delft University of Technology, Department of Civil Engingineering*.

Schoonees, T., Gijón Mancheño, A., Scheres, B., Bouma, T., Silva, R., Schlurmann, T., & Schüttrumpf, H. (2019). Hard structures for coastal protection, towards greener designs. *Estuaries and Coasts*, *42*(7), 1709–1729.

Seelig, W. (1983). Wave reflection from coastal structures. *Proceedings, Coastal Structures' 83, ASCE*.

Syvitski, J. P., Vörösmarty, C. J., Kettner, A. J., & Green, P. (2005). Impact of humans on the flux of terrestrial sediment to the global coastal ocean. *science*, *308*(5720), 376–380.

Van Bemmelen, C., De Schipper, M., Darnall, J., & Aarninkhof, S. (2020). Beach scarp dynamics at nourished beaches. *Coastal Engineering*, *160*, 103725.

Van der Meer, J. W., Briganti, R., Zanuttigh, B., & Wang, B. (2005). Wave transmission and reflection at low-crested structures: Design formulae, oblique wave attack and spectral change. *Coastal Engineering*, *52*(10-11), 915–929.

Van Gent, M. R. A. (1999). *Physical model investigations on coastal structures with shallow foreshores; 2d model tests with single and double-peaked wave energy spectra* (tech. rep. No. H3608). Delft Hydraulics. Delft.

Van Gent, M. R. A. (2019). Climate adaptation of coastal structures. *Proceedings of the SCACR19—9th Short Course/Conference on Applied Coastal Research, Bari, Italy*, 9–11.

Van Gent, M. R. A., Buis, L., van den Bos, J. P., & Wüthrich, D. (2023). Wave transmission at submerged coastal structures and artificial reefs. *Coastal Engineering*, *184*, 104344.

Van Gent, M. R. A., & Teng, D. (2023). Climate adaptation of coastal structures: Application of adaptation pathways for rubble mound breakwaters. *Proc. PIANC-COPEDEC X, Manila*.

Van Gent, M. R. (2024). Submerged low-crested structures in front of coastal structures. *Journal of Coastal and Hydraulic Structures*, *4*.

Van Rijn, L. (2011). Coastal erosion and control. *Ocean & Coastal Management*, *54*(12), 867–887.

Wang, X. L., Feng, Y., & Swail, V. R. (2014). Changes in global ocean wave heights as projected using multimodel cmip5 simulations. *Geophysical Research Letters*, *41*(3), 1026–1034.

Zanuttigh, B., & Van der Meer, J. W. (2007). Wave reflection from coastal structures. In *Coastal engineering 2006: (in 5 volumes)* (pp. 4337–4349). World Scientific.

Zelt, J., & Skjelbreia, J. E. (1993). Estimating incident and reflected wave fields using an arbitrary number of wave gauges. In *Coastal engineering 1992* (pp. 777–789).

# Appendix A: Calibration of Wave Gauges

Wave Gauges are measuring instruments used in physical models to measure the wave heights and water levels. They however do not measure water levels directly. Instead the data measured by the wave gauges are in the unit of voltages. The magnitude of the voltage measured depends on the depth of the water column that exists above the probe of the wave gauge. The taller the water column above the probe the higher or more positive the measured voltage. In order to subsequently convert the voltage values into water depths, a calibration coefficient specific to each wave gauge is required. The calibration coefficient is in the units of (Volts/meter) and represents the change in volts measured for every meter change in the depth of the water column above the probe. The process of determining the calibration coefficient is as follows:

1. Set the water level in the flume to a known level and note down the measured voltage by the wave gauge
2. Repeat the previous setup for different water levels
3. Fit a linear regression line across the measured pairs of value
4. The slope of the regression line is the calibration coefficient

The calibration coefficients for Wave Gauges 1 to 9 can be found in Table A.1 below.

Table A.1: Calibration coefficients for the wave gauges used to convert voltage measurements to water surface elevation.

| Wave gauge | Calibration coefficient (m/V) |
|---|---|
| WG1 | 0.0244 |
| WG2 | 0.0249 |
| WG3 | 0.0239 |
| WG4 | 0.0254 |
| WG5 | 0.0250 |
| WG6 | 0.0249 |
| WG7 | 0.0249 |
| WG8 | 0.0259 |
| WG9 | 0.0254 |

# B

# Appendix B: Go Pro Camera Settings

Table B.1: GoPro camera settings used during the experiments.

| Setting | Option |
|---|---|
| Resolution / Frames per second | 1080p / 60 FPS |
| Lens | Linear |
| Hypersmooth | Off |
| Scheduled Capture | Off |
| Duration | No limit (manual stop) |
| Hindsight | Off |
| Timer | Off |
| Zoom | 1.0x |
| Bitrate | Low |
| Shutter | Auto |
| EV Comp | 0 |
| White Balance | Auto |
| ISO Min | 100 |
| ISO Max | 1600 |
| Sharpness | Medium |
| Colour | Natural |
| Raw Audio | Off |
| Wind | Auto |
| Media Mod | - |

C

# Appendix C: Calculation of Artificial Reef Porosity

The porosity of the reef was estimated using the following method.

1. Weigh the entire reef.
    - $G = 390\ kg$
2. Calculate the total volume of the reef based on geometrical design, $V$.
    - Cross sectional area, $A = 0.308\ m^2$
    - Thickness of reef = Width of wave flume, $t = 0.76\ m$
    - Geometric volume, $V = A * t = 0.308\ * 0.76 = 0.234\ m^3$
3. Calculate the bulk density of the reef $\rho_b$.
    - $\rho_b = G/V = 390/0.234 = 1667\ kg/m^3$
4. Rock density $\rho_0 = 2800\ kg/m^3$.
5. Calculate porosity, $n$
    - $n = 1 - \rho_b/\rho_0 = 1 - 1667/2800 = 0.405$

# Appendix D: Log sheet of Physical Model Tests

In the log sheet, each run is identified by unique test ID in the form of

$$position\_H_{m0}\_s_{m-1,0}\_R_c\_T_p\_duration$$

For example a test labelled as 1_008_0015_-0150_203_34 meant that it was carried out with

- the reef at position 1
- a significant wave height of 0.08 m
- a wave steepness of 0.015
- a freeboard of -0.150 m
- a peak period of 2.03 seconds
- a generated wave sequence of 34 minutes.

## Log sheet for Position 1 tests

Table D.1: Test log for Position 1

| No. | Test ID | $H_s$ (m) | $s_{m-1,0}$ | $R_c$ (m) | $T_p$ (s) | Duration (min) |
|---|---|---|---|---|---|---|
| 1 | 1_008_0015_0000_203_34 | 0.08 | 0.015 | 0.000 | 2.03 | 34 |
| 2 | 1_008_0015_-0050_203_34 | 0.08 | 0.015 | -0.050 | 2.03 | 34 |
| 3 | 1_008_0015_-0075_203_34 | 0.08 | 0.015 | -0.075 | 2.03 | 34 |
| 4 | 1_008_0015_-0100_203_34 | 0.08 | 0.015 | -0.100 | 2.03 | 34 |
| 5 | 1_008_0015_-0125_203_34 | 0.08 | 0.015 | -0.125 | 2.03 | 34 |
| 6 | 1_008_0015_-0150_203_34 | 0.08 | 0.015 | -0.150 | 2.03 | 34 |
| 7 | 1_008_0025_0000_157_26 | 0.08 | 0.025 | 0.000 | 1.57 | 26 |
| 8 | 1_008_0025_-0050_157_26 | 0.08 | 0.025 | -0.050 | 1.57 | 26 |
| 9 | 1_008_0025_-0075_157_26 | 0.08 | 0.025 | -0.075 | 1.57 | 26 |
| 10 | 1_008_0025_-0100_157_26 | 0.08 | 0.025 | -0.100 | 1.57 | 26 |
| 11 | 1_008_0025_-0125_157_26 | 0.08 | 0.025 | -0.125 | 1.57 | 26 |
| 12 | 1_008_0025_-0150_157_26 | 0.08 | 0.025 | -0.150 | 1.57 | 26 |
| 13 | 1_008_0040_0000_124_21 | 0.08 | 0.040 | 0.000 | 1.24 | 21 |

*Continued on next page*

Test log for Position 1 (continued)

| No. | Test ID | $H_s$ (m) | $s_{m-1,0}$ | $R_c$ (m) | $T_p$ (s) | Duration (min) |
|---|---|---|---|---|---|---|
| 14 | 1_008_0040_-0050_124_21 | 0.08 | 0.040 | -0.050 | 1.24 | 21 |
| 15 | 1_008_0040_-0075_124_21 | 0.08 | 0.040 | -0.075 | 1.24 | 21 |
| 16 | 1_008_0040_-0100_124_21 | 0.08 | 0.040 | -0.100 | 1.24 | 21 |
| 17 | 1_008_0040_-0125_124_21 | 0.08 | 0.040 | -0.125 | 1.24 | 21 |
| 18 | 1_008_0040_-0150_124_21 | 0.08 | 0.040 | -0.150 | 1.24 | 21 |
| 19 | 1_012_0015_0000_249_41 | 0.12 | 0.015 | 0.000 | 2.49 | 41 |
| 20 | 1_012_0015_-0050_249_41 | 0.12 | 0.015 | -0.050 | 2.49 | 41 |
| 21 | 1_012_0015_-0075_249_41 | 0.12 | 0.015 | -0.075 | 2.49 | 41 |
| 22 | 1_012_0015_-0100_249_41 | 0.12 | 0.015 | -0.100 | 2.49 | 41 |
| 23 | 1_012_0015_-0125_249_41 | 0.12 | 0.015 | -0.125 | 2.49 | 41 |
| 24 | 1_012_0015_-0150_249_41 | 0.12 | 0.015 | -0.150 | 2.49 | 41 |
| 25 | 1_012_0025_0000_193_32 | 0.12 | 0.025 | 0.000 | 1.93 | 32 |
| 26 | 1_012_0025_-0050_193_32 | 0.12 | 0.025 | -0.050 | 1.93 | 32 |
| 27 | 1_012_0025_-0075_193_32 | 0.12 | 0.025 | -0.075 | 1.93 | 32 |
| 28 | 1_012_0025_-0100_193_32 | 0.12 | 0.025 | -0.100 | 1.93 | 32 |
| 29 | 1_012_0025_-0125_193_32 | 0.12 | 0.025 | -0.125 | 1.93 | 32 |
| 30 | 1_012_0025_-0150_193_32 | 0.12 | 0.025 | -0.150 | 1.93 | 32 |
| 31 | 1_012_0040_0000_152_25 | 0.12 | 0.040 | 0.000 | 1.52 | 25 |
| 32 | 1_012_0040_-0050_152_25 | 0.12 | 0.040 | -0.050 | 1.52 | 25 |
| 33 | 1_012_0040_-0075_152_25 | 0.12 | 0.040 | -0.075 | 1.52 | 25 |
| 34 | 1_012_0040_-0100_152_25 | 0.12 | 0.040 | -0.100 | 1.52 | 25 |
| 35 | 1_012_0040_-0125_152_25 | 0.12 | 0.040 | -0.125 | 1.52 | 25 |
| 36 | 1_012_0040_-0150_152_25 | 0.12 | 0.040 | -0.150 | 1.52 | 25 |
| 37 | 1_016_0015_0000_288_48 | 0.16 | 0.015 | 0.000 | 2.88 | 48 |
| 38 | 1_016_0015_-0050_288_48 | 0.16 | 0.015 | -0.050 | 2.88 | 48 |
| 39 | 1_016_0015_-0075_288_48 | 0.16 | 0.015 | -0.075 | 2.88 | 48 |
| 40 | 1_016_0015_-0100_288_48 | 0.16 | 0.015 | -0.100 | 2.88 | 48 |
| 41 | 1_016_0015_-0125_288_48 | 0.16 | 0.015 | -0.125 | 2.88 | 48 |
| 42 | 1_016_0015_-0150_288_48 | 0.16 | 0.015 | -0.150 | 2.88 | 48 |
| 43 | 1_016_0025_0000_223_37 | 0.16 | 0.025 | 0.000 | 2.23 | 37 |
| 44 | 1_016_0025_-0050_223_37 | 0.16 | 0.025 | -0.050 | 2.23 | 37 |
| 45 | 1_016_0025_-0075_223_37 | 0.16 | 0.025 | -0.075 | 2.23 | 37 |
| 46 | 1_016_0025_-0100_223_37 | 0.16 | 0.025 | -0.100 | 2.23 | 37 |
| 47 | 1_016_0025_-0125_223_37 | 0.16 | 0.025 | -0.125 | 2.23 | 37 |
| 48 | 1_016_0025_-0150_223_37 | 0.16 | 0.025 | -0.150 | 2.23 | 37 |
| 49 | 1_016_0040_0000_176_29 | 0.16 | 0.040 | 0.000 | 1.76 | 29 |
| 50 | 1_016_0040_-0050_176_29 | 0.16 | 0.040 | -0.050 | 1.76 | 29 |
| 51 | 1_016_0040_-0075_176_29 | 0.16 | 0.040 | -0.075 | 1.76 | 29 |
| 52 | 1_016_0040_-0100_176_29 | 0.16 | 0.040 | -0.100 | 1.76 | 29 |
| 53 | 1_016_0040_-0125_176_29 | 0.16 | 0.040 | -0.125 | 1.76 | 29 |
| 54 | 1_016_0040_-0150_176_29 | 0.16 | 0.040 | -0.150 | 1.76 | 29 |
| 55 | 1_019_0015_0000_313_52 | 0.19 | 0.015 | 0.000 | 3.13 | 52 |
| 56 | 1_019_0025_0000_243_40 | 0.19 | 0.025 | 0.000 | 2.43 | 40 |
| 57 | 1_019_0040_0000_192_32 | 0.19 | 0.040 | 0.000 | 1.92 | 32 |
| 58 | 1_020_0015_-0050_321_54 | 0.20 | 0.015 | -0.050 | 3.21 | 54 |
| 59 | 1_020_0015_-0075_321_54 | 0.20 | 0.015 | -0.075 | 3.21 | 54 |
| 60 | 1_020_0015_-0100_321_54 | 0.20 | 0.015 | -0.100 | 3.21 | 54 |
| 61 | 1_020_0015_-0125_321_54 | 0.20 | 0.015 | -0.125 | 3.21 | 54 |
| 62 | 1_020_0015_-0150_321_54 | 0.20 | 0.015 | -0.150 | 3.21 | 54 |
| 63 | 1_020_0025_-0050_249_41 | 0.20 | 0.025 | -0.050 | 2.49 | 41 |
| 64 | 1_020_0025_-0075_249_41 | 0.20 | 0.025 | -0.075 | 2.49 | 41 |
| 65 | 1_020_0025_-0100_249_41 | 0.20 | 0.025 | -0.100 | 2.49 | 41 |

*Continued on next page*

Test log for Position 1 (continued)

| No. | Test ID | $H_s$ (m) | $s_{m-1,0}$ | $R_c$ (m) | $T_p$ (s) | Duration (min) |
|---|---|---|---|---|---|---|
| 66 | 1_020_0025_-0125_249_41 | 0.20 | 0.025 | -0.125 | 2.49 | 41 |
| 67 | 1_020_0025_-0150_249_41 | 0.20 | 0.025 | -0.150 | 2.49 | 41 |
| 68 | 1_020_0040_-0050_197_33 | 0.20 | 0.040 | -0.050 | 1.97 | 33 |
| 69 | 1_020_0040_-0075_197_33 | 0.20 | 0.040 | -0.075 | 1.97 | 33 |
| 70 | 1_020_0040_-0100_197_33 | 0.20 | 0.040 | -0.100 | 1.97 | 33 |
| 71 | 1_020_0040_-0125_197_33 | 0.20 | 0.040 | -0.125 | 1.97 | 33 |
| 72 | 1_020_0040_-0150_197_33 | 0.20 | 0.040 | -0.150 | 1.97 | 33 |

# Log sheet for Position 2 tests

Table D.2: Test log for Position 2

| No. | Test ID | $H_s$ (m) | $s_{m-1,0}$ | $R_c$ (m) | $T_p$ (s) | Duration (min) |
|---|---|---|---|---|---|---|
| 1 | 2_012_0015_0000_249_31 | 0.12 | 0.015 | 0.000 | 2.49 | 31 |
| 2 | 2_012_0015_-0050_249_31 | 0.12 | 0.015 | -0.050 | 2.49 | 31 |
| 3 | 2_012_0015_-0100_249_31 | 0.12 | 0.015 | -0.100 | 2.49 | 31 |
| 4 | 2_012_0015_-0150_249_31 | 0.12 | 0.015 | -0.150 | 2.49 | 31 |
| 5 | 2_012_0025_0000_193_24 | 0.12 | 0.025 | 0.000 | 1.93 | 24 |
| 6 | 2_012_0025_-0050_193_24 | 0.12 | 0.025 | -0.050 | 1.93 | 24 |
| 7 | 2_012_0025_-0100_193_24 | 0.12 | 0.025 | -0.100 | 1.93 | 24 |
| 8 | 2_012_0025_-0150_193_24 | 0.12 | 0.025 | -0.150 | 1.93 | 24 |
| 9 | 2_012_0040_0000_152_19 | 0.12 | 0.040 | 0.000 | 1.52 | 19 |
| 10 | 2_012_0040_-0050_152_19 | 0.12 | 0.040 | -0.050 | 1.52 | 19 |
| 11 | 2_012_0040_-0100_152_19 | 0.12 | 0.040 | -0.100 | 1.52 | 19 |
| 12 | 2_012_0040_-0150_152_19 | 0.12 | 0.040 | -0.150 | 1.52 | 19 |
| 13 | 2_016_0015_0000_288_44 | 0.16 | 0.015 | 0.000 | 2.88 | 44 |
| 14 | 2_016_0015_-0050_288_44 | 0.16 | 0.015 | -0.050 | 2.88 | 44 |
| 15 | 2_016_0015_-0100_288_44 | 0.16 | 0.015 | -0.100 | 2.88 | 44 |
| 16 | 2_016_0025_0000_223_34 | 0.16 | 0.025 | 0.000 | 2.23 | 34 |
| 17 | 2_016_0025_-0050_223_34 | 0.16 | 0.025 | -0.050 | 2.23 | 34 |
| 18 | 2_016_0025_-0100_223_34 | 0.16 | 0.025 | -0.100 | 2.23 | 34 |
| 19 | 2_016_0040_0000_176_27 | 0.16 | 0.040 | 0.000 | 1.76 | 27 |
| 20 | 2_016_0040_-0050_176_27 | 0.16 | 0.040 | -0.050 | 1.76 | 27 |
| 21 | 2_016_0040_-0100_176_27 | 0.16 | 0.040 | -0.100 | 1.76 | 27 |
| 22 | 2_020_0015_0000_321_49 | 0.20 | 0.015 | 0.000 | 3.21 | 49 |
| 23 | 2_020_0015_-0050_321_49 | 0.20 | 0.015 | -0.050 | 3.21 | 49 |
| 24 | 2_020_0015_-0100_321_49 | 0.20 | 0.015 | -0.100 | 3.21 | 49 |
| 25 | 2_020_0025_0000_249_38 | 0.20 | 0.025 | 0.000 | 2.49 | 38 |
| 26 | 2_020_0025_-0050_249_38 | 0.20 | 0.025 | -0.050 | 2.49 | 38 |
| 27 | 2_020_0025_-0100_249_38 | 0.20 | 0.025 | -0.100 | 2.49 | 38 |
| 28 | 2_020_0040_0000_197_30 | 0.20 | 0.040 | 0.000 | 1.97 | 30 |
| 29 | 2_020_0040_-0050_197_30 | 0.20 | 0.040 | -0.050 | 1.97 | 30 |
| 30 | 2_020_0040_-0100_197_30 | 0.20 | 0.040 | -0.100 | 1.97 | 30 |

# Log sheet for Position 3 tests

Table D.3: Test log for Position 3

| No. | Test ID | $H_s$ (m) | $s_{m-1,0}$ | $R_c$ (m) | $T_p$ (s) | Duration (min) |
|---|---|---|---|---|---|---|
| 1 | 3_012_0015_-0050_249_41 | 0.12 | 0.015 | -0.050 | 2.49 | 41 |
| 2 | 3_012_0015_-0100_249_41 | 0.12 | 0.015 | -0.100 | 2.49 | 41 |
| 3 | 3_012_0015_-0150_249_41 | 0.12 | 0.015 | -0.150 | 2.49 | 41 |
| 4 | 3_012_0025_-0050_193_32 | 0.12 | 0.025 | -0.050 | 1.93 | 32 |
| 5 | 3_012_0025_-0100_193_32 | 0.12 | 0.025 | -0.100 | 1.93 | 32 |
| 6 | 3_012_0025_-0150_193_32 | 0.12 | 0.025 | -0.150 | 1.93 | 32 |
| 7 | 3_012_0040_-0050_152_25 | 0.12 | 0.040 | -0.050 | 1.52 | 25 |
| 8 | 3_012_0040_-0100_152_25 | 0.12 | 0.040 | -0.100 | 1.52 | 25 |
| 9 | 3_012_0040_-0150_152_25 | 0.12 | 0.040 | -0.150 | 1.52 | 25 |
| 10 | 3_016_0015_-0050_288_48 | 0.16 | 0.015 | -0.050 | 2.88 | 48 |
| 11 | 3_016_0015_-0100_288_48 | 0.16 | 0.015 | -0.100 | 2.88 | 48 |
| 12 | 3_016_0015_-0150_288_48 | 0.16 | 0.015 | -0.150 | 2.88 | 48 |
| 13 | 3_016_0025_-0050_223_37 | 0.16 | 0.025 | -0.050 | 2.23 | 37 |
| 14 | 3_016_0025_-0100_223_37 | 0.16 | 0.025 | -0.100 | 2.23 | 37 |
| 15 | 3_016_0025_-0150_223_37 | 0.16 | 0.025 | -0.150 | 2.23 | 37 |
| 16 | 3_016_0040_-0050_176_29 | 0.16 | 0.040 | -0.050 | 1.76 | 29 |
| 17 | 3_016_0040_-0100_176_29 | 0.16 | 0.040 | -0.100 | 1.76 | 29 |
| 18 | 3_016_0040_-0150_176_29 | 0.16 | 0.040 | -0.150 | 1.76 | 29 |
| 19 | 3_018_0015_-0050_305_51 | 0.18 | 0.015 | -0.050 | 3.05 | 51 |
| 20 | 3_018_0025_-0050_236_39 | 0.18 | 0.025 | -0.050 | 2.36 | 39 |
| 21 | 3_018_0040_-0050_187_31 | 0.18 | 0.040 | -0.050 | 1.87 | 31 |
| 22 | 3_020_0015_-0100_321_54 | 0.20 | 0.015 | -0.100 | 3.21 | 54 |
| 23 | 3_020_0015_-0150_321_54 | 0.20 | 0.015 | -0.150 | 3.21 | 54 |
| 24 | 3_020_0025_-0100_249_41 | 0.20 | 0.025 | -0.100 | 2.49 | 41 |
| 25 | 3_020_0025_-0150_249_41 | 0.20 | 0.025 | -0.150 | 2.49 | 41 |
| 26 | 3_020_0040_-0100_197_33 | 0.20 | 0.040 | -0.100 | 1.97 | 33 |
| 27 | 3_020_0040_-0150_197_33 | 0.20 | 0.040 | -0.150 | 1.97 | 33 |